eEF2 in the prefrontal cortex promotes excitatory synaptic transmission and social novelty behavior

Xuanyue Ma[1,†] (ID), Liuren Li[1,†] (ID), Ziming Li[2,†] (ID), Zhengyi Huang[1] (ID), Yaorong Yang[1] (ID), Peng Liu[1] (ID), Daji Guo[1,3] (ID), Yueyao Li[1] (ID), Tianying Wu[1] (ID), Ruixiang Luo[1] (ID), Junyu Xu[4] (ID), Wen-Cai Ye[1,5,6,*] (ID), Bin Jiang[2,**] (ID) & Lei Shi[1,5,6,***] (ID)

Abstract

Regulation of mRNA translation is essential for brain development and function. Translation elongation factor eEF2 acts as a molecular hub orchestrating various synaptic signals to protein synthesis control and participates in hippocampus-dependent cognitive functions. However, whether eEF2 regulates other behaviors in different brain regions has been unknown. Here, we construct a line of *Eef2* heterozygous (HET) mice, which show a reduction in eEF2 and protein synthesis mainly in excitatory neurons of the prefrontal cortex. The mice also show lower spine density, reduced excitability, and AMPAR-mediated synaptic transmission in pyramidal neurons of the medial prefrontal cortex (mPFC). While HET mice exhibit normal learning and memory, they show defective social behavior and elevated anxiety. Knockdown of *Eef2* in excitatory neurons of the mPFC specifically is sufficient to impair social novelty preference. Either chemogenetic activation of excitatory neurons in the mPFC or mPFC local infusion of the AMPAR potentiator PF-4778574 corrects the social novelty deficit of HET mice. Collectively, we identify a novel role for eEF2 in promoting prefrontal AMPAR-mediated synaptic transmission underlying social novelty behavior.

Introduction

Protein synthesis (mRNA translation) is one of the most crucial steps that determine the cellular proteome (Schwanhäusser *et al*, 2011; Dong *et al*, 2020). Owing to the extensive polarized structure of brain cells, including both nerve and glial cells, protein synthesis is usually regulated locally in different cellular compartments and is highly arranged in a cell type-specific manner, which adds more complex layers to the mRNA translational regulation in the brain comparing to other organs (Holt *et al*, 2019). Protein synthesis is known to control almost every aspect of brain development and circuit wiring, ranging from neurogenesis/morphogenesis to synapse formation/plasticity (Park *et al*, 2021; Sossin, 2021). Not surprisingly, accumulating evidence has demonstrated protein synthesis as a vulnerable site for attack in a variety of neurological diseases, including neurodevelopmental disorders, mood disorders, and neurodegenerative disorders (Delaidelli *et al*, 2019; Sossin & Costa-Mattioli, 2019; Laguesse & Ron, 2020; Sossin, 2021). Hence, understanding the mRNA translational control machinery is critical for deciphering the mechanisms of brain health and disease.

Eukaryotic elongation factor 2 (eEF2), a unique factor that regulates the phase of mRNA translation elongation, catalyzes the GTP-dependent translocation of peptidyl tRNA from the A site to the P site of ribosome, thus making ribosome to shift along the reading frame of mRNA with polypeptide elongation. Missense variations of *EEF2* or defective post-translation modification of the protein have been found causatively linked with neurodevelopmental disorders and spinocerebellar ataxia (Hekman *et al*, 2012; Hawer *et al*, 2020; Nabais Sá *et al*, 2021). The best studied molecular regulation of eEF2 activity is through inhibitory phosphorylation at Thr56 (pT56) by eEF2 kinase (eEF2K), also known as Ca^{2+}/calmodulin-dependent protein kinases III (CaMKIII). It has been revealed that eEF2K quickly senses different forms of synaptic plasticity and antidepressants such as Ketamine

1 JNU-HKUST Joint Laboratory for Neuroscience and Innovative Drug Research, College of Pharmacy, Jinan University, Guangzhou, China
2 Guangdong Province Key Laboratory of Brain Function and Disease, Zhongshan School of Medicine, Sun Yat-sen University, Guangzhou, China
3 Clinical Neuroscience Institute, The First Affiliated Hospital of Jinan University, Guangzhou, China
4 Department of Neurobiology and Department of Rehabilitation of the Children's Hospital, Zhejiang University School of Medicine, Hangzhou, China
5 Center for Bioactive Natural Molecules and Innovative Drugs Research, College of Pharmacy, Jinan University, Guangzhou, China
6 Guangdong Province Key Laboratory of Pharmacodynamic Constituents of TCM and New Drugs Research, College of Pharmacy, Jinan University, Guangzhou, China
   *Corresponding author. Tel: +86 20 85220936; E-mail: chywc@aliyun.com
   **Corresponding author. Tel: +86 20 87331839; E-mail: jiangb3@mail.sysu.edu.cn
   ***Corresponding author. Tel: +86 20 85222120; E-mail: t_shilei@jnu.edu.cn or E-mail: sophielshi80@gmail.com
   †These authors contributed equally to this work

(Sutton *et al*, 2007; Park *et al*, 2008; Adaikkan *et al*, 2018; Zanos & Gould, 2018; David *et al*, 2020; Ghosh Dastidar *et al*, 2020), thereby leading to the dephosphorylation and activation of eEF2 (Verpelli *et al*, 2010; Heise *et al*, 2014). The most studied role of eEF2K-eEF2 pathway in animals is in the hippocampus, where it regulates synaptic transmission, neurogenesis, and cognition (Gosrani *et al*, 2020; Taha *et al*, 2020). Using eEF2K knockout mice as a model, these studies conclude that eEF2K could be a detrimental factor to a number of hippocampal-dependent forms of learning and memory, whereas activation of eEF2 by eEF2K suppression facilitates cognition. Consistently, eEF2K activity is found to increase in several neurodegenerative conditions, and deletion or pharmacological inhibition of eEF2K enhances cognition in Alzheimer and Parkinson mouse models (Jan *et al*, 2017, 2018; Beckelman *et al*, 2019; Ma, 2021; Yang *et al*, 2021b).

Nonetheless, most of the above studies used eEF2K deficiency models, which leads to several unsolved aspects for eEF2 itself. First, evidence is missing regarding how the physiological level of eEF2 regulates brain development and function from direct loss-of-function manipulations of eEF2. Given that other possible mechanisms exist to control the ribosome translocation activity of eEF2 (Shen *et al*, 2021), observations from eEF2K models may not be necessarily sufficient to predict eEF2 function. Second, the spatiotemporal expression of eEF2 in different brain regions and different neuronal types has not been fully investigated. In this regard, eEF2 may have essential roles in regulating the functioning of different brain regions and related behaviors. Unraveling these functions of eEF2 is important for the understanding of mRNA translation elongation control in brain function and disease.

In the current study, we first characterized the spatiotemporal expression of eEF2 in the brain, revealing a higher expression of eEF2 in excitatory neurons. Using CRISPR/Cas9 strategy, we constructed a heterozygous *Eef2*-deleted mouse line (*Eef2* HET mice), which showed a specific reduction of eEF2 protein and lowered *de novo* protein synthesis in the prefrontal cortex (PFC). Spine abnormalities and lowered synaptic GluA2 component were observed, along with decreased excitability and impaired AMPAR-mediated synaptic transmission in Layer 5 neurons of medial PFC (mPFC). Intriguingly, the HET mice exhibited social and communication deficits, stereotyped behavior, and elevated anxiety. Further study showed that *Eef2* knockdown in the excitatory neurons of mPFC was sufficient to cause abnormal social novelty preference. Using the chemogenetic approach, we demonstrated that enhancing the excitability of these mPFC pyramidal neurons rescued the social novelty behavior in *Eef2* HET mice. Finally, either systematic or mPFC local administration of the AMPAR potentiator PF-4778574 successfully corrected the social novelty deficit of the HET mice. Collectively, these findings uncover a previously unrecognized role of prefrontal eEF2 in regulating AMPAR-mediated synaptic transmission and social novelty behavior.

Results

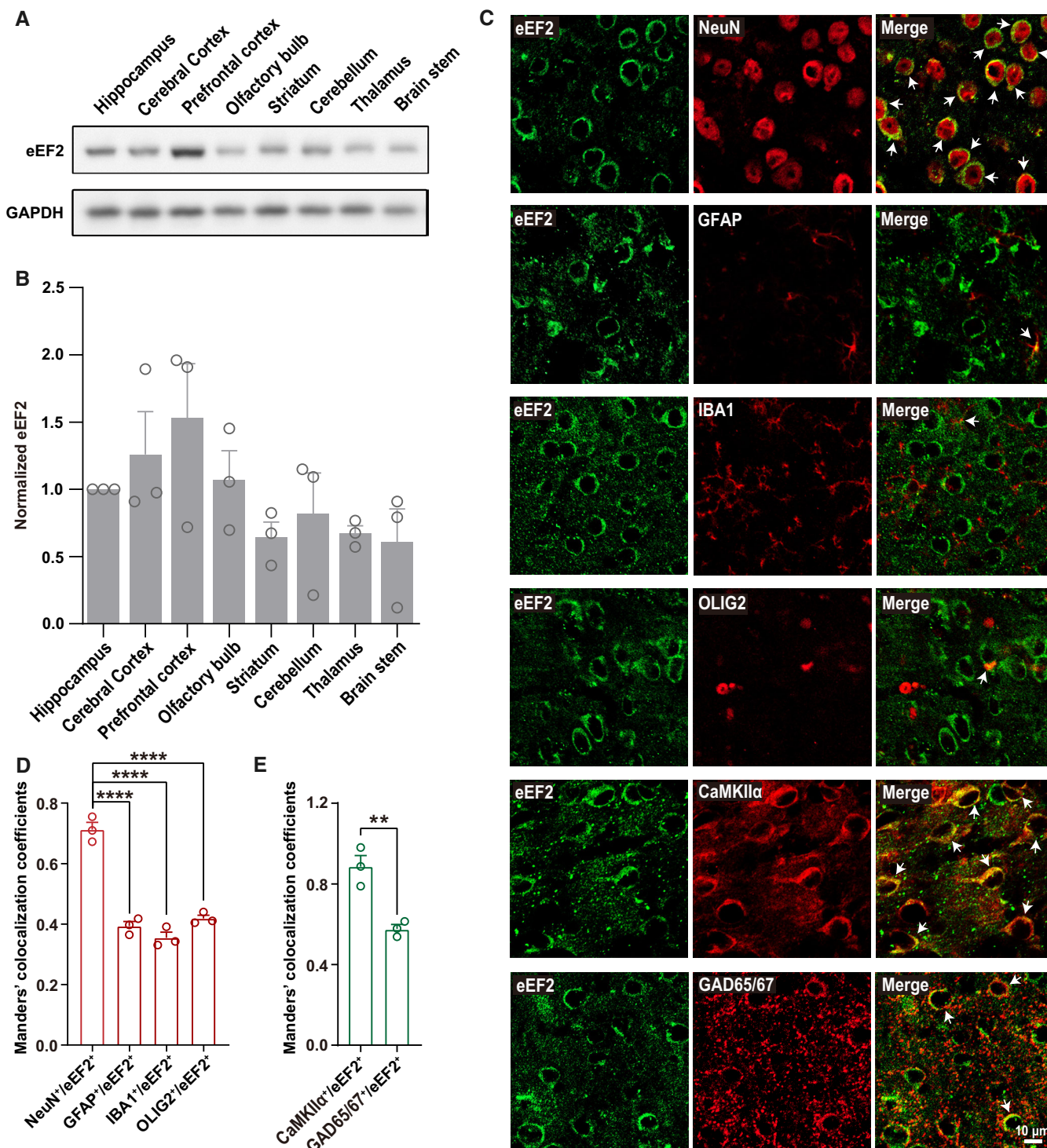### eEF2 is highly expressed in the excitatory neurons in mouse brain

We revealed that eEF2 is widely expressed in various brain regions, with relatively higher expression in the cerebral cortex, in particular the PFC, and hippocampus (Fig 1A and B). To show the cellular subtype distribution of eEF2, we examined the colocalization of eEF2 with markers of different cell types in both the cortex and hippocampus (Figs 1C, and EV1A and B), including NeuN (a marker of neurons), GFAP (glial fibrillary acidic protein; a marker of astrocytes), IBA1 (ionized calcium-binding adaptor molecule 1; a marker of microglia), OLIG2 (oligodendrocyte lineage transcription factor 2; a marker of oligodendrocytes), CaMKIIα (Ca^{2+}/calmodulin-dependent protein kinase IIα; a marker of excitatory neurons), and GAD65/67 (glutamic-acid decarboxylase 65 and 67; markers of GABAergic inhibitory neurons). eEF2 has much higher expression in neuronal cells than in glial cells (Figs 1D and EV1C). Moreover, the colocalization of eEF2 with CaMKIIα was significantly higher than with GAD65/67 (Figs 1E and EV1D), suggesting that relative more eEF2 is localized to excitatory neurons than inhibitory neurons. The specificity of the immunoreactivity of eEF2 primary antibody was verified (Fig EV1E). Thus, eEF2 is widely distributed in different brain regions with the highest expression in the excitatory neurons.

Reduced eEF2 leads to lowered protein synthesis in the excitatory neurons of prefrontal cortex

Although eEF2 has been suggested for participating in various processes of neuronal development, most studies have focused on the role of eEF2K and the consequent pT56-eEF2, thus lacking direct evidence of eEF2 deficiency. To directly investigate the function of eEF2, we constructed an *Eef2* knockout mouse line by CRISPR/Cas9 strategy for studying its *in vivo* role in brain function and behavior (Fig 2A). Notably, no *Eef2* null embryos were detected even as early as E11.5, suggesting a failure of embryo formation or very early embryonic lethality by homozygous deletion of *Eef2* (Fig EV2A and B). Although the mortality rate of HET embryos appeared higher than WT ones at gestation stages, the survived HET mice exhibited normal growth rate (weight gain) and normal gross brain architecture (Fig EV2C–I). We verified that gene editing of *Eef2* was successful in different brain regions (Fig EV2J), and the *Eef2* mRNA levels were reduced significantly in the cortex (without PFC), PFC, hippocampus, and striatum of HET mice (Fig EV3A–D). However, the eEF2 protein levels only showed a significant reduction (~30%) in the PFC, a reduction trend in the hippocampus, but no change in the rest part of the cortex or the striatum of the HET mice (Fig 2B and C).

We further confirmed the reduction of eEF2 in HET PFC by immunostaining (Fig EV3E). The fluorescence intensity of eEF2 and the number of eEF2-positive cells were both significantly decreased in the mPFC of the HET mice (Fig EV3F and G). By analyzing eEF2 expression in different neuronal types, we showed that eEF2 was specifically reduced in CaMKIIα-positive excitatory neurons, but not GAD65/67-positive inhibitory neurons in the mPFC of the HET mice (Fig 2D–G). As eEF2 functions to promote protein synthesis, we examined whether the reduced eEF2 in the HET PFC leads to reduced protein synthesis. Surface sensing of translation (SUnSET)-based measurement was performed to verify that *de novo* global protein synthesis was evidently reduced in the PFC, but not in the rest part of the cortex and the hippocampus of the HET mice (Figs 2H and I, and EV4A and B). Furthermore, using the methionine analog azidohomoalanine (AHA) as a non-canonical amino acid to label newly synthesized proteins, we found that the AHA

Figure 1. eEF2 is highly expressed in the excitatory neurons in mouse brain.

A   Western blots of eEF2 expression in different brain regions, GAPDH was used as a loading control.

B   eEF2 expression levels were quantified and represented as fold changes of that in the hippocampus. $n = 3$ mice for each brain region.

C   Immunofluorescent staining of eEF2 (green) and different nervous system cells (red: NeuN/GFAP/IBA1/OLIG2/CaMKIIα/GAD65/67) in the somatosensory cortex of adult mice brains. Arrows indicate highly colocalized cells. Scale bar, 10 μm.

D, E   Colocalization of eEF2 and each cellular marker was quantified by calculating the Manders' colocalization coefficients. Six slices from three mice in each condition. (D) One-way ANOVA with Bonferroni's multiple comparison *post hoc*, ****$P < 0.0001$ (NeuN[+]/eEF2[+] versus GFAP[+]/eEF2[+]), ****$P < 0.0001$ (NeuN[+]/eEF2[+] versus IBA1^{+}/eEF2[+]), ****$P < 0.0001$ (NeuN[+]/eEF2[+] versus OLIG2^{+}/eEF2[+]). (E) Unpaired *t* test, **$P = 0.0065$ (CaMKIIα[+]/eEF2[+] versus GAD65/67[+]/eEF2[+]).

Data information: All data are shown as mean ± s.e.m. All the *t* tests are two-tailed.
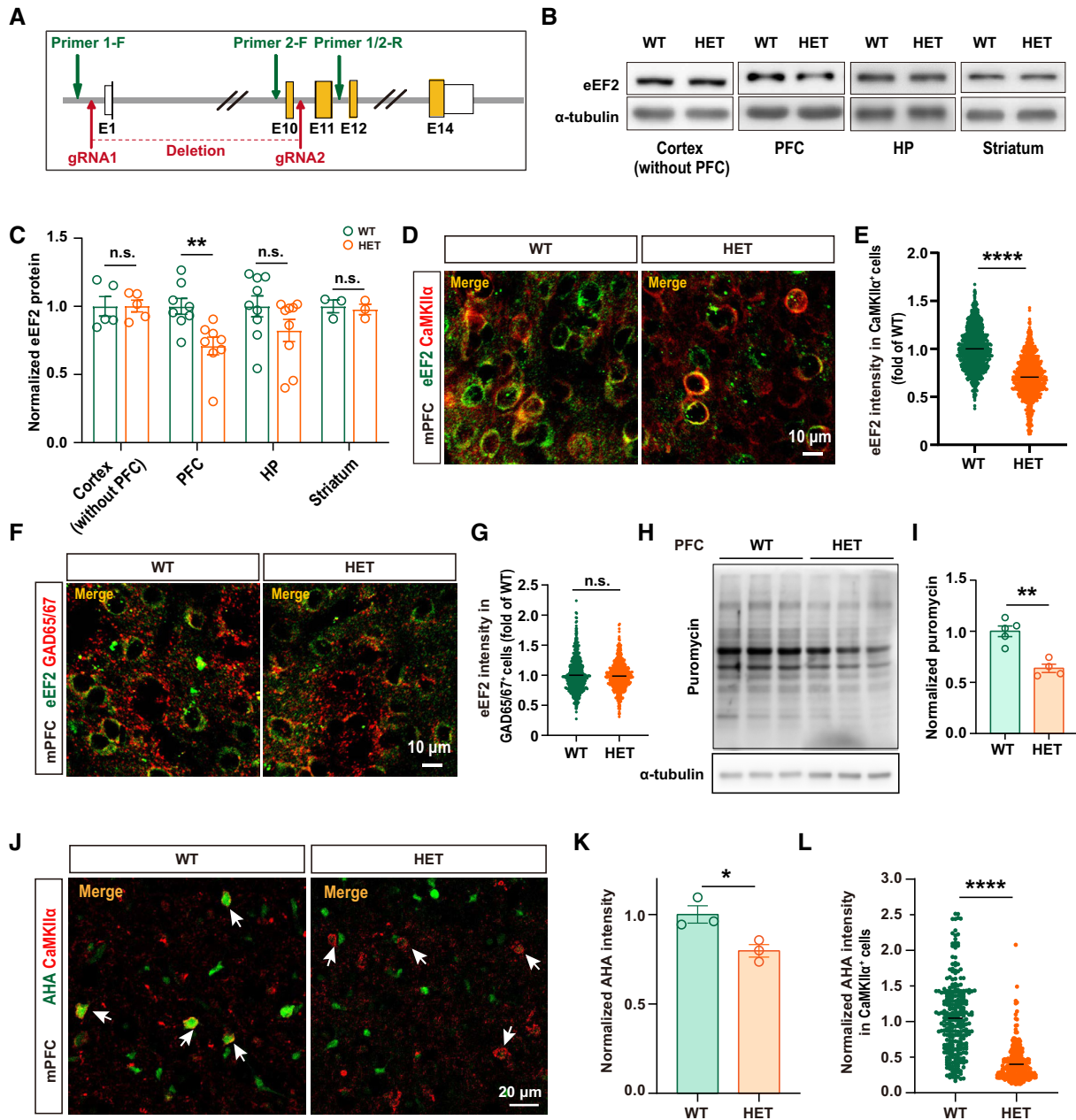
Figure 2. Reduced eEF2 protein level and decreased protein synthesis in excitatory neurons of the prefrontal cortex in *Eef2* HET mice.

A   A schematic showing the CRISPR/Cas9 strategy used to delete *Eef2*.

B   Western blots of eEF2 in the PFC, the rest part of the cortex, the hippocampus, and the striatum of *Eef2* WT and HET mice.

C   Quantification analysis of (B). $n = 5$ mice for the cortex (without PFC), $n = 8$ mice for PFC, $n = 9$ mice for HP, $n = 3$ mice for striatum. Unpaired t tests. Cortex (without PFC), $P = 0.9757$; PFC, **$P = 0.0049$; HP, $P = 0.1338$; Striatum, $P = 0.7301$.

D   Representative merged immunofluorescent staining images of eEF2 (green) and CaMKIIα (red) in the mPFC of *Eef2* WT and HET mice. Scale bar, 10 μm.

E   Quantification of mean fluorescent intensity of eEF2 in CaMKIIα$^+$ cells in WT and HET mPFC. $n = 918$ cells from 3 WT mice, $n = 965$ cells from 3 HET mice. Unpaired t test. ****$P < 0.0001$.

F   Representative merged immunofluorescent staining images of eEF2 (green) and GAD65/67 (red) in the mPFC of *Eef2* WT and HET mice. Scale bar, 10 μm.

G   Quantification of mean fluorescent intensity of eEF2 in GAD65/67$^+$ cells in WT and HET mPFC. $n = 690$ cells from 3 WT mice, $n = 686$ cells from 3 HET mice. Mann–Whitney test. $P = 0.6757$.

H   Western blots of *de novo* global protein synthesis in PFC slices of WT and HET mice, measured by SUnSET. α-tubulin was used as a loading control.

I   Quantification analysis of puromycin-labeled protein levels. WT, $n = 5$ mice, HET, $n = 4$ mice. Unpaired t tests. **$P = 0.0011$.

J   Representative images of AHA incorporation (green) with CaMKIIα$^+$ staining (red) in mPFC of WT and HET mice. Arrows indicate CaMKIIα$^+$ cells. Scale bar, 20 μm.

K   Quantification of total AHA incorporation. Twelve slices from three mice for each genotype. Unpaired t test. *$P = 0.0268$.

L   Quantification of AHA incorporation in CaMKIIα$^+$ cells. $n = 276$ cells from 3 WT mice, $n = 293$ cells from 3 HET mice. Mann–Whitney test. ****$P < 0.0001$.

Data information: All data are shown as mean ± s.e.m. All the tests are two-tailed.

incorporation levels were significantly reduced in the mPFC of the HET mice, which may be mainly contributed by the reduction in CaMKIIα-positive excitatory neurons (Fig 2J–L). Together, the *Eef2* HET mice constructed in this study exhibit a specific reduction of eEF2 protein with a concomitant protein synthesis decrease mainly in the excitatory neurons of PFC.

Altered proteome and reduced number of excitatory synapses in the prefrontal cortex of *Eef2* HET mice

To investigate whether the lower protein synthesis in the HET PFC leads to protein expression changes at the synapse, we performed liquid chromatography–mass spectrometry (LC–MS)/MS-based proteomic analysis in crude synaptosome preparations from the PFC of WT and HET mice (Fig 3A). Principal component analysis (PCA) for total 3,957 quantified proteins showed close clustering of replicates but clear segregation between WT and HET samples (Fig 3B). The top 15% of up- or downregulated proteins were represented in a heatmap, which showed an obvious alteration in the synaptic proteome of HET mice (Fig 3C). Gene Ontology (GO) analysis on these proteins revealed that proteins involved in translation, including both mitochondrial translation and cytosolic translation, were downregulated, which was consistent with the decreased protein synthesis in the PFC of HET mice. Besides, proteins involved in synapse function, including those in regulating postsynaptic membrane neurotransmitter receptor levels, receptor-mediated endocytosis, synapse organization, and cytoskeleton, were also downregulated in PFC synaptosome fractions of HET mice (Fig 3D and Dataset EV1). Interestingly, the upregulated proteins were enriched in translational initiation, structural constituent of ribosome, nucleic acid transport, RNA splicing, and protein stabilization, perhaps indicating a compensatory regulation in the translation mechanism (Fig 3E and Dataset EV1). To further investigate the altered processes in PFC synaptosome induced by *Eef2* reduction, we utilized Gene Set Enrichment Analysis (GSEA) to analyze whether the gene sets of the above highlighted GO terms show a difference between HET and WT groups. Similar to GO enrichment, the mitochondrial translation-, actin binding-, and cell adhesion-related proteins were significantly enriched in downregulated sets in the HET samples (Fig 3F). We verified that the levels of cytoskeletal regulators CDC42, RHOA, PAK1 were altered in PFC synaptosome of *Eef2* HET mice. Moreover, the autism-associated proteins FMR1, ELMO1, and CYFIP1, and the synaptic protein synaptophysin, were changed in the synaptosome by eEF2 reduction (Fig EV4C and D).

These proteomic changes may indicate an altered synaptic structure in the PFC. To this end, we analyzed the number of dendritic spines, where the excitatory synapses reside. Indeed, the spine density was reduced significantly in the pyramidal neurons of HET mPFC (Fig 3G and H). We next examined the expressions of different subunits of AMPARs and NMDARs, the most widely-present excitatory synaptic receptors. Of note, the AMPAR subunit GluA2, but not GluA1, was reduced significantly in the synaptosome preparations of the HET PFC (Fig 3I and J). NMDAR subunits GluN1 and GluN2B levels were not altered at the synapse, but GluN2B showed a decreasing trend (Fig 3I and J). The mRNA levels of all these receptor subunits were unchanged in the HET PFC (Appendix Fig S1), suggesting that these proteins were not affected at the transcription level. Given the role of eEF2 in mRNA translation regulation, it is highly possible that the reduction in GluA2 in eEF2 knockdown neurons is caused by decreased mRNA translation. To test this hypothesis, we performed the proximity ligation assay (PLA) to examine the level of *de novo* synthesized GluA2 in cortical neurons infected by *Eef2* shRNA-expressing lentivirus (Fig 3K). Indeed, there was a remarkable decline of newly synthesized GluA2 protein in *Eef2* knockdown neurons (Fig 3L–N and Appendix Fig S2). Together, eEF2 efficiency led to altered synaptic proteome, reduced spine density, and decreased synaptic level of GluA2 in the PFC of the HET mice.

Figure 3. Altered proteome and reduced number of excitatory synapses in the prefrontal cortex of *Eef2* HET mice.

A PFC, indicated by the boxed area, was examined for LC–MS/MS for synaptosome proteome.

B Principal component analysis (PCA) of all quantified data sets of PFC synaptosome proteome. Green triangles and orange circles represent WT and HET samples, respectively.

C A heatmap of expression levels of top 15% altered proteins in all samples.

D, E Gene ontology (GO) enrichment analysis for top 15% altered proteins of WT and HET samples. Bubble charts showed main biological process (BP) and molecular function (MF) terms with significant enrichment (*P*-value < 0.05, FDR < 0.25) from downregulated (D) and upregulated (E) proteins.

F Gene Set Enrichment Analysis (GSEA) was performed to analyze expression cohorts from WT and HET PFC synaptosome. Enrichment plots of the GO mitochondrial translation gene set (NES = −1.56, FDR = 0.010), actin-binding gene set (NES = −1.28, FDR = 0.023), and cell adhesion gene set (NES = −1.20, FDR = 0.080) were shown. NES, normalized enrichment score.

G Representative images of Golgi-stained dendrite spines in the mPFC from WT and HET mice. Scale bar, 5 μm.

H Quantification of spine density per 10 μm of dendrites. n = 18 dendrites from 3 WT mice; n = 23 dendrites from 3 HET mice. Unpaired t test. ****P < 0.0001.

I Representative Western blots of expression levels of AMPAR and NMDAR subunits in the synaptosomal fraction of WT and HET PFC. α-tubulin was served as a loading control.

J Quantification analysis of synaptosomal expression of different receptor subunits. Unpaired t test. GluA1, P = 0.9346; GluA2, **P = 0.0075; GluN1, P = 0.6946; GluN2A, P = 0.4091; GluN2B, P = 0.0796. n.s.—not significant. n = 5 mice for each genotype.

K The schematic of puromycin-proximity ligation assay (PLA).

L Representative immunofluorescent images of eEF2 (magenta) and PLA signals (white) in lentivirus (LV)-scramble-EGFP or LV-*Eef2* shRNA-EGFP infected primary cortical neurons (green, DIV 14). Scale bar, 10 μm.

M Quantification of mean fluorescent intensity of eEF2 in EGFP+ cells in scramble and *Eef2* shRNA groups. Sixty-four cells for scramble group and 51 cells for *Eef2* shRNA group from three independent experiments. Mann–Whitney test. ****P < 0.0001.

N Quantification of mean fluorescent intensity of PLA signals in EGFP+ cells in the two groups. The PLA signals represent newly synthesized GluA2. Sixty-four cells for scramble group, 51 cells for *Eef2* shRNA group from three independent experiments. Mann–Whitney test. ****P < 0.0001.

Data information: All data are shown as mean ± s.e.m. All the tests are two-tailed.
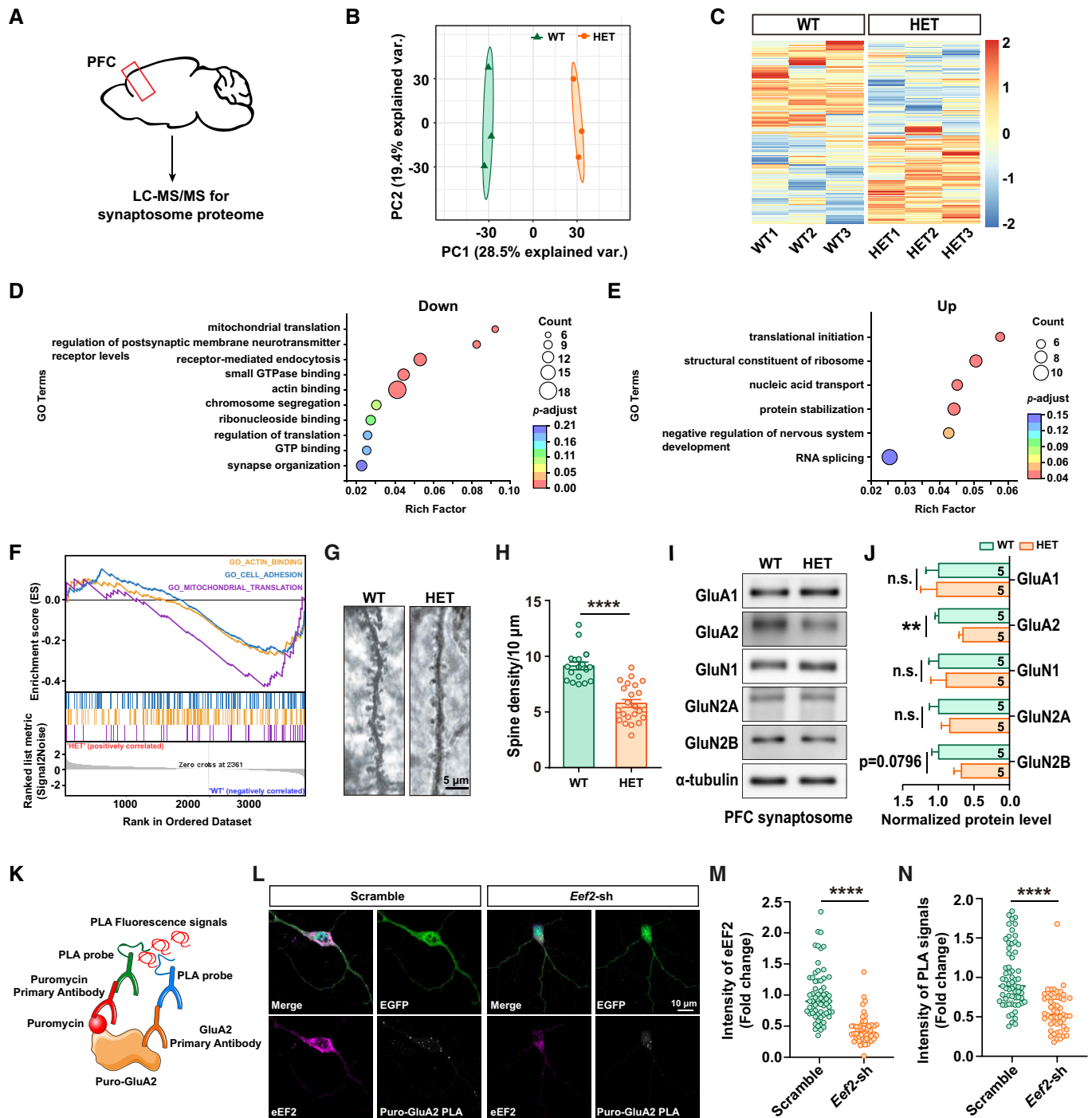
Figure 3.

Impaired AMPAR-mediated synaptic transmission of mPFC pyramidal neurons in *Eef2* HET mice

To examine whether the synaptic transmission is changed in the HET mPFC, we applied whole-cell recordings on Layer 5 pyramidal neurons in the prelimbic cortex (PrL), one of the major output neurons of mPFC (Fig 4A). The action potential firing rate induced by current injection was significantly lower in HET neurons than WT

neurons, suggesting lowered excitability of the mutant neurons (Fig 4B and C). Furthermore, the excitatory postsynaptic current (EPSC) amplitude was found to decrease notably (Fig 4D and E), whereas the inhibitory postsynaptic current (IPSC) amplitude remained intact (Fig 4D and F), leading to a reduction of excitation/ inhibition (E/I) ratio in these HET neurons (Fig 4G). To explore the cause of decreased excitatory input of the mutant neurons, we differentially measured AMPAR- and NMDAR-mediated evoked EPSCs

Figure 4.

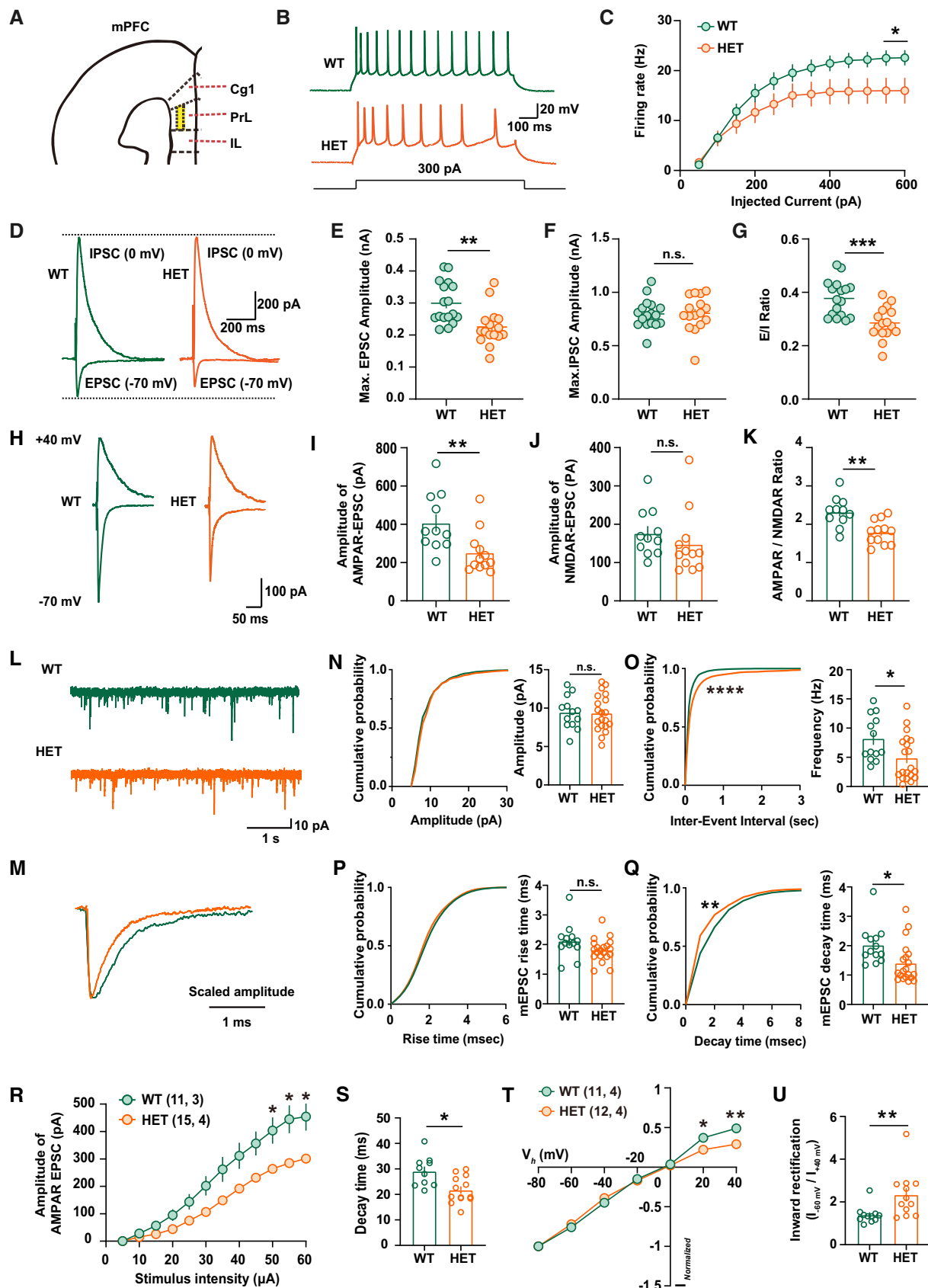**Figure 4. Impaired AMPAR-mediated synaptic transmission of mPFC pyramidal neurons in *Eef2* HET mice.**

A   A depiction of Layer 5 (L5) prelimbic region of mPFC (yellow area), which is the target region for electrophysiological recordings in this study.

B   Representative traces of action potential from WT and HET mice by current injection at 300 pA.

C   Averaged firing rates of L5 pyramid neurons, induced by 50 pA step-current injections (0–600 pA). WT (24 cells, 4 mice), HET (27 cells, 4 mice). Unpaired *t* test, *P = 0.046.

D   Representative traces of evoked EPSC and IPSC in the same L5 pyramidal cells of PrL from WT and HET mice.

E, F   The maximal EPSC (E) and IPSC (F) recorded from WT (17 cells, 6 mice) and HET (16 cells, 6 mice) groups. Unpaired *t* test, **P = 0.0016 (E) and P = 0.9296 (F).

G   The E/I ratio was reduced in HET mice. Unpaired *t* test, ***P = 0.0002.

H   Representative traces of AMPAR/NMDAR-EPSC from WT and HET mice.

I–K   AMPAR-EPSC in L5 cells is reduced in HET mice, unpaired *t* test, **P = 0.0100 (I), but NMDAR-EPSC is unchanged, unpaired *t* test, P = 0.3681 (J), resulting in reduced AMPAR/NMDAR ratio, unpaired *t* test, **P = 0.0014 (K). WT: 11 cells, 4 mice; HET: 12 cells, 4 mice.

L, M   Representative (L) and average (M) traces of mEPSCs in WT and HET L5 pyramidal cells.

N–Q   Cumulative probabilities and averaged values of mEPSC amplitude (N), inter-event interval/frequency (O), rise time (P), and decay time (Q) in WT (13 cells, 4 mice) and HET (20 cells, 4 mice) groups. For cumulative probabilities, two-sample Kolmogorov–Smirnov test, P = 0.1361 (N); ****P = 0.0001 (O); P = 0.999 (P); **P = 0.0082 (Q). For averaged values, unpaired *t* test, P = 0.9068 (N); *P = 0.0197 (O); P = 0.0872 (P); *P = 0.0160 (Q).

R   The EPSC evoked in L5 neurons has a smaller amplitude in HET than in WT mice. 25–30% decrease at strongest stimulation (10 cells from 3 WT mice, 13 cells from 4 HET mice), unpaired *t* test, *P = 0.0279.

S   Quantification of decay time, 10 cells from 3 WT mice, 13 cells from 4 HET mice, unpaired *t* test. *P = 0.0047.

T   Inward rectification in WT and HET mice (11 cells from 4 WT mice; 12 cells from 4 HET mice), unpaired *t* test, *P = 0.0393 at +20 mV; **P = 0.016 at +40 mV.

U   Quantification of the inward rectification, 11 cells from 4 WT mice; 12 cells from 4 HET mice, unpaired *t* test, **P = 0.0078.

Data information: All data are shown as mean ± s.e.m. n.s.—not significant. All the *t* tests are two-tailed.

in same neurons. Notably, we identified that only AMPAR-EPSCs were reduced whereas NMDAR-EPSCs were intact (Fig 4H–K) in the HET neurons. To further describe the alteration of AMPAR-mediated synaptic transmission, we recorded the AMPAR-mediated miniature EPSCs (mEPSCs) in layer 5 PrL pyramidal neurons. Interestingly, although the mEPSC amplitude was unchanged, the current decay time was significantly shortened in the HET neurons compared to the WT group (Fig 4L–Q), suggesting aberrant kinetics of AMPARs in the mutant neurons. Moreover, the mEPSC frequency was smaller in HET neurons than in WT neurons (Fig 4O), which may be resulted from decreased presynaptic input or reduced number of AMPAR-containing synapses. We further confirmed that the peak amplitude and the decay time of AMPAR-EPSCs evoked by different stimulation intensities were significantly lower in HET neurons than those in WT mice (Fig 4R and S, and Appendix Fig S3A). As we observed declined expression of GluA2 but unaltered GluA1, we measured the inward rectification of AMPARs characteristic by a shift of synaptic AMPAR composition into a smaller GluA2-to-GluA1 ratio. Indeed, we recorded an increase in the inward rectification in HET neurons (Fig 4T and U, and Appendix Fig S3B), suggesting that a reduced fraction of GluA2-containing AMPARs is present at the synapse resulting from eEF2 reduction. Together, these data indicate that eEF2 is indispensable for maintaining normal AMPAR-mediated synaptic transmission in the mPFC.

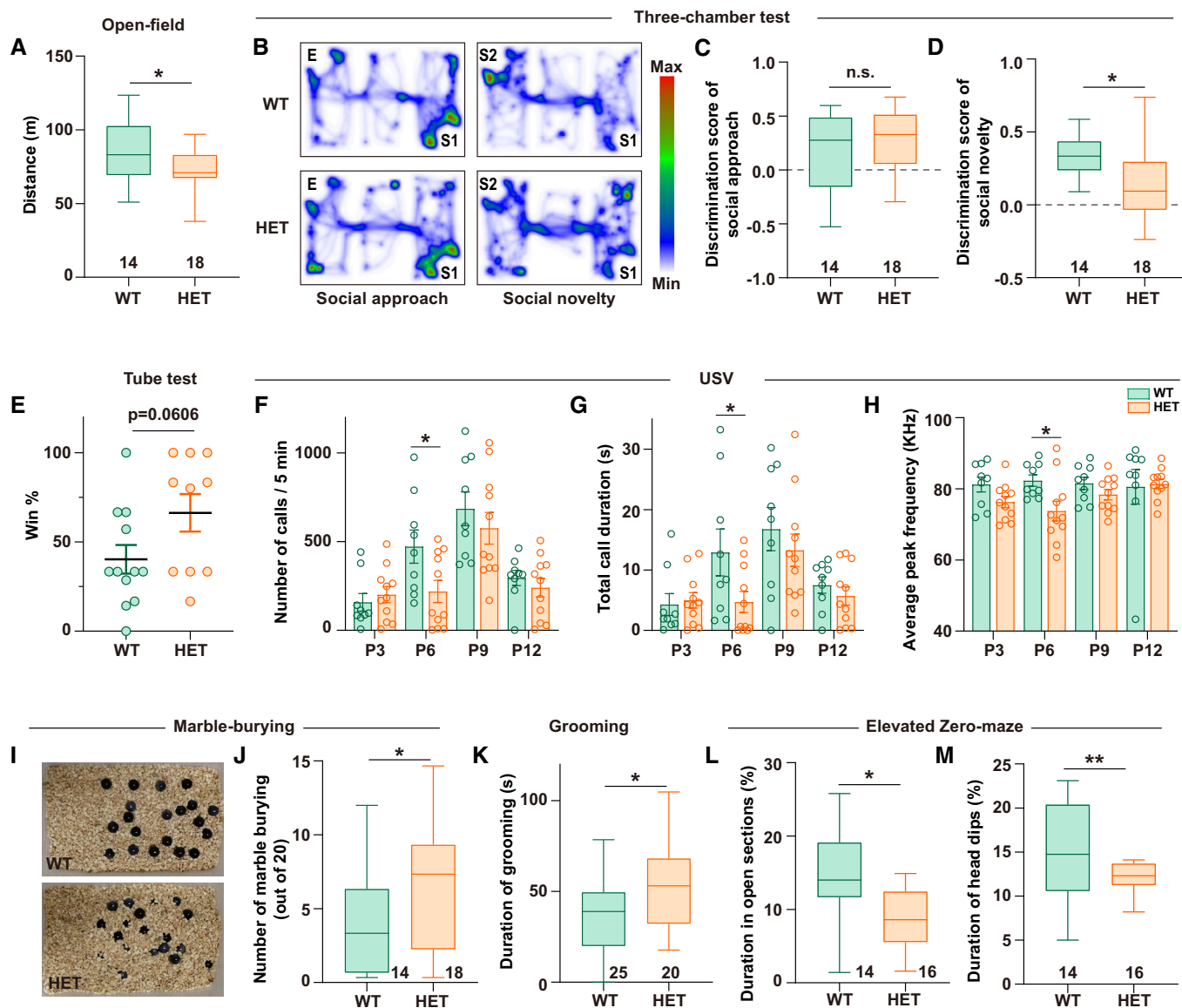### *Eef2* HET mice exhibit social deficits and elevated anxiety

As PFC is critically involved in higher cognitive and emotional function (Chini & Hanganu-Opatz, 2021), we explored how mice behaviors are influenced by the abnormalities in the PFC of *Eef2* HET mice. A battery of behavior tests was run on *Eef2* HET mice, including spontaneous exploration, nesting, learning and memory, social and communication behaviors, and anxiety/depression levels. In the open-field test, HET mice traveled a slightly shorter distance than the WT group, suggesting a reduction in spontaneous exploration (Fig 5A). The nesting behavior, the object recognition memory, and the Y-maze alternation-based working memory were

normal in the HET mice (Fig EV5A–E). Intriguingly, however, the HET mice exhibit a series of social and emotional abnormalities.

In the three-chamber sociability and social novelty test, the HET mice displayed a normal discrimination score on sniffing a stranger conspecific over an inanimate object (Fig 5B and C). However, they failed to distinguish a novel conspecific from a familiar one, showing impaired social novelty preference (Fig 5D). In another social test, the tube test, which is a classical model to assess the social dominance hierarchy, the HET mice had a greater percentage of wins when they contended with the WT mice of matched sex, age, and weight, suggesting that the HET mice showed stronger social aggression than WT mice (Fig 5E). Having found that the HET mice exhibited social deficits based on body behaviors, we examined another aspect of social function, the social language communication. Ultrasonic vocalizations (USVs) of mouse pups were recorded and analyzed during the isolation from their dam on different developmental days during the first two postnatal weeks, in which USVs show a peak between postnatal day (P) 6 and P9 (Hahn *et al*, 1998; Hahn & Schanz, 2002). Notably, the total number of calls was significantly reduced in HET pups when comparing with their WT littermates at P6, along with shortened duration, lowered peak frequency of calls, and declined duration of the longest call (Figs 5F–H and EV5F). These results collectively suggest that impaired social interaction and communication are among the key behavioral features of *Eef2* HET mice. Interestingly, the HET mice also exhibit a characteristic stereotyped repetitive behavior with increased marble burying and grooming (Fig 5I–K).

We then examined whether emotional levels are altered in the HET mice. First, the anxiety level was evaluated using the Elevated Zero-maze (EZM). We found that the HET mice spent less time traveling in the open sections than the WT mice (Figs 5L and EV5G). Moreover, the HET mice did not place their heads outside the edge of open corridors (an activity known as head dips) as often as the WT mice did (Fig 5M), indicative of reduced exploratory activity of HET mice. These results suggest that the *Eef2* HET mice exhibit anxiety-like behavior. Second, as eEF2 has been known to mediate the fast antidepressant effect of Ketamine (Adaikkan *et al*, 2018;

Figure 5. *Eef2* HET mice show social deficits and elevated anxiety.

A   Travel distance of WT and *Eef2* HET mice in the Open-field test. WT, *n* = 14 mice; HET, *n* = 18 mice. Unpaired *t* test. *P = 0.0390.

B   Heatmaps of the two social tasks (left, social approach; right, social novelty) of the three-chamber test performed by mice of different genotypes. E: empty cup; S1: stranger #1 contained cup; S2: stranger #2 contained cup.

C   Discrimination score of social approach of WT and HET mice, calculated by the difference of time spent in sniffing S1 and E. WT, *n* = 14 mice; HET, *n* = 18 mice. Unpaired *t* test. P = 0.3947.

D   Discrimination score of social novelty of WT and HET mice, calculated by the difference of time spent in sniffing S2 and S1. WT, *n* = 14 mice; HET, *n* = 18 mice. Welch's *t* test. *P = 0.0306.

E   Social dominance evaluation of WT and HET mice in the tube test, quantified as the percentage of win numbers. WT, *n* = 12 mice; HET, *n* = 10 mice. Mann–Whitney test. P = 0.0606.

F–H   Three evaluation parameters of isolation-induced pup ultrasonic vocalizations (USVs) at different postnatal days (P3, P6, P9, P12). WT, *n* = 9 pups; HET, *n* = 11 pups. (F) Number of calls during 5-min recording, quantified by the Mann–Whitney test, *P = 0.0465 at P6. (G) Total duration of calls analyzed by the Mann–Whitney test. *P = 0.0465 at P6. (H) Average peak frequency of calls, unpaired *t* test. *P = 0.0209 at P6. No significance (P > 0.05) at P3, P9, and P12 between WT and HET mice in all three measurements.

I   The representative images of the marble-burying test.

J   Statistics of the number of marbles buried by WT and HET mice. WT, *n* = 14 mice; HET, *n* = 18 mice. Mann–Whitney test. *P = 0.0417.

K   Time spent for grooming during 20-min test of WT and HET mice. WT, *n* = 25 mice; HET, *n* = 20 mice. Unpaired *t* test. *P = 0.0436.

L, M   Elevated Zero-maze was used to test anxiety-like behavior. WT, *n* = 14 mice; HET, *n* = 16 mice. (L) Duration spent in open sections by WT and HET mice, analyzed by unpaired *t* test. *P = 0.0124. (M) Duration of head dips in open sections performed by WT and HET mice. Kolmogorov–Smirnov test, **P = 0.0042.

Data information: Data of (E–H) are shown as mean ± s.e.m., data of (A, C, D, and J–M) are shown as an interquartile range, with a line across the box indicating median, whiskers show the highest and lowest values. n.s.—not significant. All the *t* tests and Mann–Whitney tests are two-tailed.

Zanos & Gould, 2018), we examined the acute depression levels induced by the despair from the forced-swim test. However, the HET mice showed no changes in the duration of immobility, escaping, climbing, and swimming (Fig EV5H–K), suggesting a lack of depression-associated behavior. Collectively, eEF2 reduction in the PFC led to a set of social abnormalities including impaired social novelty preference, increased social aggression, and altered vocal communication, accompanied by increased repetitive stereotypes and elevated anxiety.

eEF2 in excitatory neurons of mPFC regulates social novelty behavior

As we have found that the *Eef2* HET mice showed eEF2 reduction mainly in the excitatory neurons of mPFC, we asked whether the behavioral abnormalities are generated by eEF2 insufficiency in these cells. We bilaterally injected adeno-associated virus (AAV) expressing either CMV-DIO-EGFP-*Eef2* shRNA or CMV-DIO-EGFP-scramble shRNA into the mPFC of CaMKIIα-Cre mice, to achieve *Eef2* knockdown specifically in the excitatory neurons of mPFC (Fig 6A). We confirmed that the EGFP signals were distributed in CaMKIIα$^+$ cells, but not GAD65/67$^+$ cells, at all layers of PrL, Cg1 (cingulate cortex 1), and the majority of IL (infralimbic cortex; Fig 6B). The knockdown efficiency of *Eef2* shRNA was confirmed by immunofluorescent staining, which showed marked reduction of eEF2 in *Eef2* shRNA-expressing cells (Fig 6C). Notably, reduced expression of eEF2 specifically in the excitatory neurons of mPFC was enough to impair social novelty behavior (Fig 6D–F).

To further investigate whether the lowered excitation of mPFC excitatory neurons is responsible for the altered social novelty behavior in *Eef2* HET mice, we employed the DREADDs (Designer Receptors Exclusively Activated by Designer Drugs)-based chemogenetic approach to activate these mutant neurons and then investigated whether the social novelty deficit could be corrected in the HET mice (Fig 6G). The EGFP-tagged CaMKIIα-driven excitatory hM3D (Gq) DREADD AAV was bilaterally injected into the mPFC of

the HET mice (Fig 6G). After 2-week viral infection, hM3D-expressed neurons were activated by chronic administration of the DREADD ligand clozapine N-oxide (CNO) at a low dose (0.025 mg/ml) in the drinking water for another 14 days (Fig 6H). We confirmed that the EGFP was accurately expressed at PrL, Cg1, and IL (Fig 6I), and these EGFP-positive neurons were recorded in current-clamp mode to successfully generate more action potentials triggered by the application of CNO, indicative of potentiated excitability (Appendix Fig S4). Without affecting the spontaneous exploratory locomotion (Appendix Fig S5), CNO administration notably restored social novelty preference in *Eef2* HET mice (Fig 6J–L), suggesting that normalization of the activity of mPFC excitatory neurons was sufficient for correcting impaired social novelty preference generated by eEF2 reduction. These results collectively provide direct evidence that eEF2 in mPFC excitatory neurons regulates social novelty behavior.

Pharmacological activation of AMPAR rescues social novelty deficit in *Eef2* HET mice

As the AMPAR-mediated synaptic transmission is reduced with lowered GluA2 fraction in the HET mPFC, we examined whether enhancing AMPAR function could correct the social novelty deficits in the HET mice. We used PF-4778574, a brain-penetrable AMPAR positive allosteric modulator (PAM) that has the ability to activate GluA2 (Shaffer *et al*, 2013; Shen *et al*, 2019), to test our hypothesis. Application of PF-4778574 (10 or 20 μM) directly increased both amplitude and decay time of AMPAR currents in mPFC layer 5 pyramidal neurons in brain slices from *Eef2* HET mice (Fig 7A–C and Appendix Fig S6). Moreover, the input–output response of AMPAR-EPSCs in mutant neurons was rescued by PF-4778574, showing enhanced AMPAR-EPSC amplitudes at different stimulus intensities (Fig 7D). It has been shown that PF-4778574 has a rapid effect on correcting social novelty defect in mouse models (Shen *et al*, 2019; Jabarin *et al*, 2021). Prompted by these studies, we performed a single-dose intraperitoneal administration of PF-4778574 (0.3 mg/

Figure 6. eEF2 in excitatory neurons of mPFC regulates social novelty behavior.

A CMV-DIO-EGFP-*Eef2* shRNA or CMV-DIO-EGFP-scramble adeno-associated virus (AAV) was injected into bilateral mPFC of CaMKIIα-Cre mice.

B Validation of AAV expression in mPFC CaMKIIα$^+$ cells. Scale bars, 500 μm (left) and 20 μm (right). Arrows indicate CaMKIIα$^+$ cells, and arrowheads indicate GAD65/67$^+$ cells.

C Validation of eEF2 knockdown efficiency in mPFC CaMKIIα$^+$ cells. Scale bar, 10 μm.

D Representative heatmaps of the two social tasks (left, social approach; right, social novelty) performed by mice with eEF2 knockdown in mPFC excitatory neurons in the three-chamber test. E: empty cup; S1: stranger #1 contained cup; S2: stranger #2 contained cup.

E Discrimination score of social approach of AAV-*Eef2* shRNA or AAV-scramble injected mice, calculated by the difference of time spent in sniffing S1 and E. Unpaired *t* test, *P* = 0.6442. Scramble group, *n* = 8 mice; *Eef2*-sh group, *n* = 9 mice.

F Discrimination score of social novelty performed by two groups of mice, calculated by the difference of time spent in sniffing S2 and S1. Unpaired *t* test, *P* = 0.0448. Scramble group, *n* = 8 mice; *Eef2*-sh group, *n* = 9 mice.

G EGFP-tagged CaMKIIα-driven excitatory hM3D (Gq) adeno-associated virus (AAV) was bilaterally injected into mPFC of HET mice.

H Schematic diagram of DREADDs-based experimental strategy in HET mice.

I Validation of hM3D (Gq) AAV expression in the mPFC. Scale bar, 500 μm.

J Representative heatmaps of the two social tasks (left, social approach; right, social novelty) performed by *Eef2* HET mice with oral administration of CNO or H$_2$O (served as the control) in the three-chamber test. E: empty cup; S1: stranger #1 contained cup; S2: stranger #2 contained cup.

K Discrimination score of social approach of CNO- or H$_2$O-treated mice, calculated by the difference of time spent in sniffing S1 and E. *n* = 14 mice for each group. Unpaired *t* test, *P* = 0.1999.

L Discrimination score of social novelty performed by two groups of mice, calculated by the difference of time spent in sniffing S2 and S1. Unpaired *t* test, *P* = 0.0423. *n* = 14 mice for each group.

Data information: Data are shown as an interquartile range, with line across the box indicating median, whiskers show the highest and lowest values. n.s.—not significant. All the tests are two-tailed.

Figure 6.

kg) in the HET mice and examined their social behavior in the three-chamber test 30 min later. As we proposed, PF-4778574 effectively corrected abnormal social novelty preference in the HET mice without interrupting sociability (Fig 7E–G). To eliminate the influences on peripheral organs and other brain regions by systemic administration of PF-4778574, we applied local infusion of PF-4778574 (20 μM) in bilateral mPFC through the implanted cannula (Fig 7H). Importantly, local activation of AMPAR in mPFC by PF-4778574 also rescued social novelty deficit in HET mice (Fig 7I–K). Collectively, these findings suggest that eEF2 in the mPFC modulates social novelty behavior via the regulation of AMPAR function.

Discussion

Dysregulation of mRNA translation is associated with a variety of neurological diseases. However, the mRNA translation elongation is among the least understood processes of mRNA translation in terms of whether it has a brain region-specific control pattern of behaviors. In the current study, we identified a novel role of eEF2 in regulating social novelty behavior through modulating AMPAR-mediated excitatory synaptic transmission in the mPFC. To our best knowledge, this is the first report elucidating the role of eEF2 in the mPFC using genetic deleted mice.

The mRNA translation elongation consists of two consecutive steps, the eEF1-dependent recruitment of selective aminoacyl-transfer RNA (tRNA) and the eEF2-dependent ribosome translocation. eEF1 is a multisubunit complex, and genetic mutations of these subunits are causatively linked to neurodevelopmental disorders and ASD (McLachlan et al, 2019). So far, several animal models of eEF1A2 and other eEF1 subunits have been generated and studied, and most of them recapitulate the clinical phenotype (Davies et al, 2017; Ugur Iseri et al, 2019; Larcher et al, 2020). Evidence from human has shown a similar association of eEF2 to neurodevelopmental disorders (Hekman et al, 2012; Hawer et al, 2020; Nabais Sá et al, 2021), strengthening the importance of mRNA translation elongation in brain development. However, eEF2 is much less studied comparing with eEF1 due to the lack of animal models. In this study, we constructed a mouse line of genetic deletion of Eef2 and provided new pieces of evidence for the physiological function of this gene. The failure of embryo formation caused by homozygous Eef2 deletion notably suggests the absolute requirement of the gene in early embryo development. Interestingly, the mRNA and protein levels of Eef2 in the brain do not fall in correlation. Although Eef2 mRNA level had a similar decrease (~50%) in PFC, cortex (without PFC), HP, and striatum of Eef2 HET mice, the eEF2 protein only showed ~30% reduction in the PFC, a declined trend in HP, and no change in the cortex (without PFC) and striatum. It has been extensively studied that protein levels are not simply reflected by their mRNA levels, as protein abundance is not solely dependent on

transcription, but also influenced by mechanisms including post-transcriptional regulation, mRNA trafficking, and local translation, posttranslational regulation, and protein turnover (Liu et al, 2016; Moritz et al, 2019). As eEF2 is by far the only known factor for ribosome translocation without compensation from other redundant factors, it is possible that a stringent mechanism must exist to ensure the protein level is not being easily attacked by sudden changes in mRNA. Given that the eEF2 level is relatively higher in PFC than in other brain regions (Fig 1A), this higher demand for eEF2 production may be more sensitive to the changes in available mRNA. Further investigations are required to decipher the underlying mechanisms of the brain-specific discrepancy between eEF2 mRNA and protein levels.

mPFC is one of the key brain subregions that control social behavior. Altered cellular architecture, synaptic transmission, and circuit wiring are frequently observed in both ASD individuals (Li et al, 2020; Trakoshis et al, 2020) and ASD animal models (Cao et al, 2018; Kelly et al, 2020; Sacai et al, 2020; Lee et al, 2021). In particular, the excitatory pyramidal neurons of mPFC are drawing great attention, as precise E/I balance of these neurons has to be maintained for normal social behavior. Previous studies have shown some evidence about how eEF2 may influence E/I balance through pharmacological inhibition or genetic deletion of eEF2K. Heise et al (2017) reported that eEF2K deletion resulted in an increase of inhibitory synaptic transmission without affecting excitatory synaptic transmission in dentate gyrus granule cells in the hippocampus. However, there are other studies showing that the inhibition of eEF2K induced a fast enhancement of excitatory synaptic transmission in CA1 pyramidal neurons (Weng et al, 2016), and genetic reduction in eEF2K restored long-term potentiation of HP CA1 neurons of AD model mice (Beckelman et al, 2019). The controversies may come from different cell populations and experimental paradigms. Different from these studies, we directly investigated eEF2 instead of eEF2K and showed that eEF2 reduction specifically attenuates EPSCs but not IPSCs of mPFC pyramidal neurons, resulting in lowered E/I ratio and excitability. Importantly, enhancing the excitability of the mutant excitatory neurons by DREADDs

---

Figure 7. Pharmacological activation of AMPAR restores social novelty preference in *Eef2* HET mice.

A   PF-4778574 (PF) directly potentiates EPSC amplitude; dashed line represents baseline value of normalized EPSC amplitude. Bottom: representative EPSC traces from baseline (1), maximal potentiation (2), and recovery (3).

B, C   Quantifications of EPSC peak amplitude (B) and decay time (C) after PF (6 cells from 3 HET mice). (B) Wilcoxon signed-rank test, *P = 0.0313 (PF vs. baseline) and P = 0.1600 (Wash out vs. baseline); (C) Paired t test, ****P < 0.0001 (PF vs. baseline) and P = 0.4423 (Wash out vs. baseline).

D   PF rescued AMPAR-EPSC in L5 neurons from HET mice. 25–30% increase at strongest stimulation (7 cells from 3 HET mice), paired t test, **P = 0.0014. Bottom: representative traces of the effects of PF on AMPAR-EPSC evoked by different stimulus intensities.

E   Representative heatmaps of the two social tasks (left, social approach; right, social novelty) in the three-chamber test performed by *Eef2* HET mice intraperitoneally administered with PF-4778574 or DMSO (vehicle control). E: empty cup; S1: stranger #1 contained cup; S2: stranger #2 contained cup.

F   Discrimination score of social approach performed by two groups of mice, calculated by the difference of time spent in sniffing S1 and E. Unpaired t test. P = 0.7335. WT, n = 9 mice; HET, n = 8 mice.

G   Discrimination score of social novelty performed by two groups of mice, calculated by the difference of time spent in sniffing S2 and S1. Unpaired t test. *P = 0.0492. WT, n = 9 mice; HET, n = 8 mice.

H   Schematic diagram of cannula implantation and PF infusion experimental strategy in HET mice.

I   Representative heatmaps of the two social tasks (left, social approach; right, social novelty) performed by *Eef2* HET mice with mPFC infusion of PF-4778574 or DMSO (vehicle control) in the three-chamber test. E: empty cup; S1: stranger #1 contained cup; S2: stranger #2 contained cup.

J   Discrimination score of social approach performed by two groups of mice, calculated by the difference of time spent in sniffing S1 and E. Unpaired t test. P = 0.3984. n = 11 mice for each group.

K   Discrimination score of social novelty performed by two groups of mice, calculated by the difference of time spent in sniffing S2 and S1. Unpaired t test. *P = 0.0489. n = 11 mice for each group.

Data information: Data of (A–D) are shown as mean ± s.e.m., data of (F, G, J, and K) are shown as an interquartile range, with line across the box indicating median, whiskers show the highest and lowest values. n.s.—not significant. All the t tests are two-tailed.
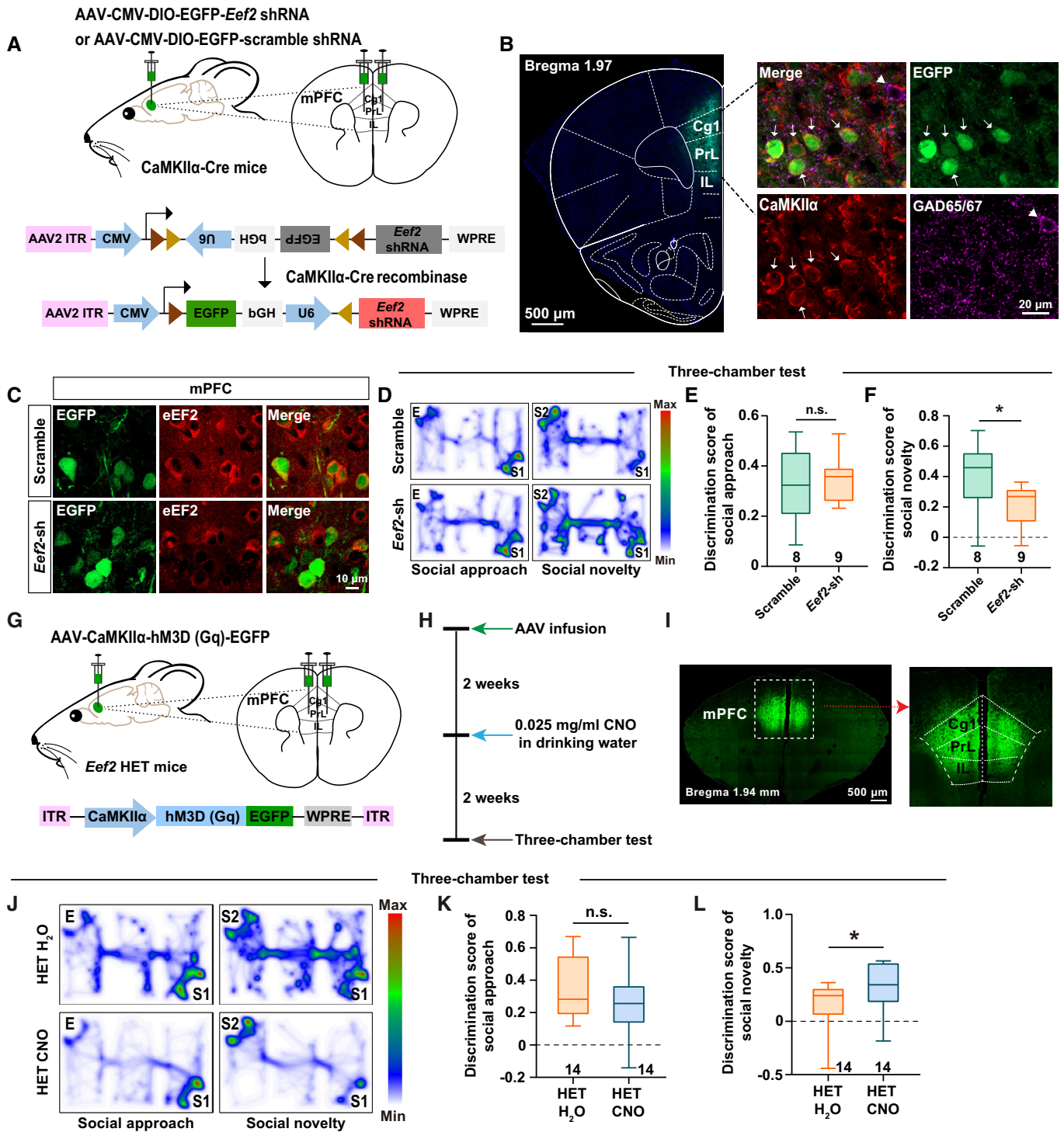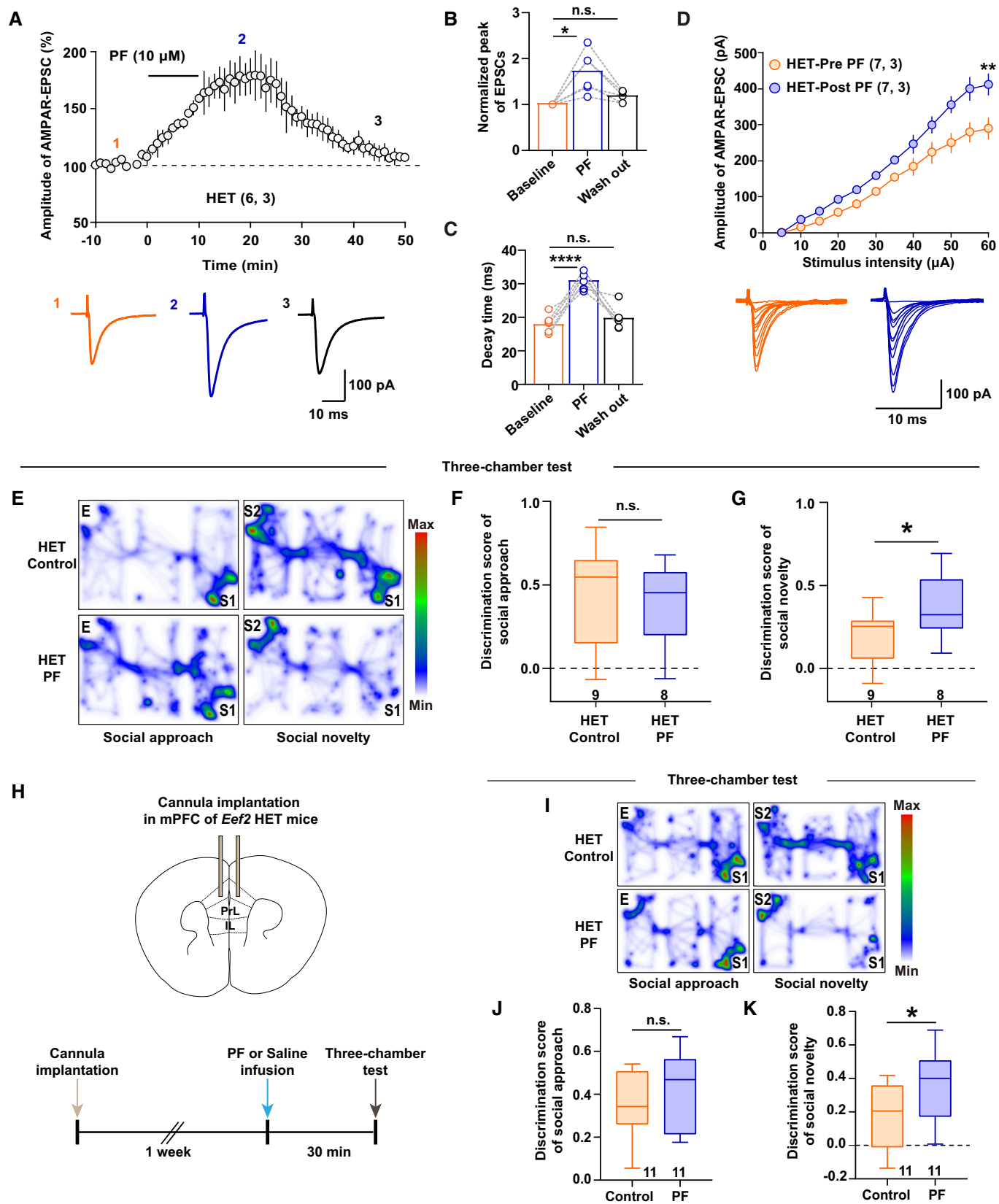
Figure 7.

chemogenetics successfully reversed the social novelty deficit in *Eef2* HET mice, further confirming the decreased excitability in HET excitatory neurons. These results are in line with observations from several ASD animal models including those with deletions of the high-risk genes *Shank3*, *Cntnap2*, or *16p11.2* (Wang *et al*, 2018; Lazaro *et al*, 2019; Qin *et al*, 2019; Sacai *et al*, 2020; Yang *et al*, 2021a), providing more evidence on the link between reduced mPFC excitation and social novelty dysfunction.

We further revealed that eEF2 reduction in mPFC specifically lowered AMPAR- but not NMDAR-mediated EPSCs. As an important therapeutic target for ASD, either hyper- or hypofunction of AMPAR could result in social novelty deficits in mice, and restoration of normal AMPAR transmission by pharmacological modulators corrects the behavioral abnormalities (Shen *et al*, 2019; Yennawar *et al*, 2019; Sacai *et al*, 2020; Jabarin *et al*, 2021). We demonstrated that the AMPAR PAM PF-4778574 potently reversed the AMPAR dysfunction and social novelty defect in *Eef2* HET mPFC. As this brain-penetrable compound also shows beneficial therapeutic effects in other ASD mice models (Shen *et al*, 2019; Jabarin *et al*, 2021), it holds the potential to be studied as a drug candidate for ASD with AMPAR pathology. Intriguingly, the impaired AMPAR function in HET mPFC was largely caused by the reduced synaptic expression of GluA2, a unique subunit of AMPAR due to its ability on calcium permeability and voltage rectification. Abnormal expression and trafficking of GluA2 affect synaptic plasticity and memory implicated in intellectual disability and Fragile X syndrome (Jia *et al*, 1996; Cook *et al*, 2014; Mignogna *et al*, 2021), and *de novo GRIA2* mutations found in individuals of neurodevelopmental disorders with ASD lead to reduced current amplitude (Salpietro *et al*, 2019). Our findings suggest that eEF2 controls the mPFC *de novo* GluA2 protein level, probably through mRNA translation elongation phase, and thereby regulating the AMPAR transmission and social novelty behavior. Besides GluA2, some actin dynamics regulatory proteins were also changed in mPFC synaptosome of *Eef2* HET mice, consistent with the decreased spine density. In addition, the translation regulatory proteins FMR1 and its interacting protein CYFIP1 were changed in the HET synaptosome, suggesting possible secondary alteration of local translation at the synapse by eEF2 reduction (Domínguez-Iturza *et al*, 2019). Whether these proteins contributed to the abnormal social novelty behavior of *Eef2* HET mice needs to be further explored.

Collectively, this study presents a new mouse model of eEF2 insufficiency and provides compelling evidence for the understanding of translation regulation of synaptic receptors in the mPFC underlying social novelty behavior.

Materials and Methods

Animals

All animal experiments were carried out in accordance with the Laboratory Animal Ethics Committee of Jinan University (IACUC Issue No: 20200325–54). *Eef2* HET mice were generated using CRISPR/Cas9 strategy. Cas9 mRNA and a pair of gRNAs (gRNA1: CATGCACAGAGCGCGGTCTT; gRNA2: GAAGGATGAGACGCCCATTC) generated by *in vitro* transcription were injected into fertilized eggs of C57BL/6 mice for deleting the genomic DNA sequence containing

the *Eef2* coding exons 1–10. The positive founders were bred to the next generation, which were used for colony breeding. Genotyping details of *Eef2* HET mice are provided as below. The CaMKIIα-Cre mice (NMX-TG-192031) were purchased from Shanghai Model Organisms Center.

Details of *Eef2* HET mice genotyping

Genotyping was determined by PCR using genomic DNA extracted from mouse tails, different brain regions including cortex (without PFC), PFC, HP, striatum, thalamus, cerebellum, and other organs including liver and spleen. WT allele was determined by a PCR product of 725 bp amplified using Primer 1-F and Primer 1/2-R; the *Eef2* null allele was determined by a PCR product of 800 bp using Primer 2-F and Primer 1/2-R. The primer sequences are as follows (from 5′ to 3′):

    Primer 1-F: CATAGGGCTGAGCCCTATGCCTG
    Primer 2-F: GTCAAATTACATAACAGTCTCAAACCCAGG
    Primer 1/2-R: GCCCTGTGAAGAGCTGGAAGTTAGAC

Embryo isolation and genotyping

The experiments were performed as described previously (Collins *et al*, 2019; Jacobs *et al*, 2020). *Eef2* heterozygous mice were intercrossed, followed by checking vaginal plugs of females at 9:00 am and 18:00 pm each day to determine the age of embryos. The day when plugs were found was determined as embryonic day 0.5. At indicated days, females were cervical dislocated and embryos were separated from the uterus in cold PBS. Yolk sac samples of death embryos and a small part of the tails of normal embryos were used for genotyping.

Protein extraction and Western blot analysis

Tissue sample homogenates and crude synaptosomes were prepared as previously described (Guo *et al*, 2021). Western blot analysis is performed using the following antibodies: eEF2 (Abcam, ab75748), pT56-eEF2 (CST, 2331S), eEF2K (CST, 3692S), Puromycin (Millipore, MABE343), GluA1 (CST, 13185S), GluA2 (Millipore, MAB397), GluN1 (Invitrogen, 320500), GluN2A (GeneTex, GTX134086), GluN2B (Millipore, 06-600), CYFIP1 (Abcam, ab6046), FMR1 (Abcam, ab17722), ELMO1 (Santa Cruz, sc-271519), ELMO2 (Santa Cruz, sc-365739), RAC1 (BD, 610650), CDC42 (CST, 2466S), RHOA (CST, 2117S), PAK1 (CST, 2602S), synaptophysin (Sigma, S5768). GAPDH (Abbkine, A01020), α-tubulin (Abbkine, A01080), β-actin (Abbkine, A01010).

RNA extraction and quantitative real-time (qRT)–PCR

After perfusing with RNase-free-DPBS treated by DEPC (Aladdin, D137738), tissues were quickly dissected out and frozen in liquid nitrogen, then homogenized in RNAiso PLUS (Takara, D9108B). cDNA was synthesized using M-MLV Reverse Transcriptase Kit (Promega, M1705). qRT–PCR was performed using SYBR Green qPCR Master Mix (Bimake, B21203) according to the manufacturer's instructions. The amplification reaction was quantified by LightCycler 480 Real-Time PCR System (Roche). The primer sequences used for qRT–PCR are as follows (from 5′ to 3′):

Eef2-RT1-F: CAGGCCATGTGGACTTCTC
Eef2-RT1-R: CTTGTTCATCATCAGGACGG
Eef2-RT2-F: CCGTCACTGCACAGAAGTAC
Eef2-RT2-R: CTACCAAAGGCATAGAAGCGG
Gapdh-F: GAGCCAAAAGGGTCATCATCTC
Gapdh-R: GTGAGCTTCCCGTTCAGCTCT
Gria1-F: AGATTGTCAGCGACGGCAA
Gria1-R: CCAAACTCATGAATGGCTTGG
Gria2-F: CCAATGGGATAAGTTCGCATACCT
Gria2-R: AGTCACCTGCCACTTCTTCTCC
Grin1-F: GGTGTCACTCACCCAACCTT
Grin1-R: ACCGGGATTAGGGGTGGTTA
Gin2a-F: TCCAGTTTGTTGGTGACGGT
Grin2a-R: GCCATGTTGTCGATGTCCAG
Grin2b-F: AGTTCCGACATTGCTTCATGG
Grin2b-R: CGGAGCAAGCGTAGGATATTG

Immunofluorescence

Mice were perfused with 4% paraformaldehyde (PFA; Sigma), post-fixed, and gradient dehydrated in 10–30% sucrose solution, followed by coronal sectioning (30 μm) on a cryostat (Leica CM1950). Brain sections were immunostained with primary antibodies at 4°C overnight and secondary antibodies at room temperature for 1 h, then incubated with DAPI for 10 min at room temperature. After being mounted with Hydromount (National Diagnostics), sections were imaged by confocal fluorescence microscopy (Zeiss LSM 800). The primary and secondary antibodies used are as follows: Anti-β-tubulin III (Sigma, T8578), Anti-GFAP (Servicebio, GB12096), Anti-eEF2 (Abcam, ab75748), Anti-NeuN (Millipore, MAB377), Anti-IBA1 (Millipore, MABN92), Anti-OLIG2 (Millipore, AB9610), Anti-CaMKIIα (Abcam, ab22609), Anti-GAD65/67 (Abcam, ab183999), Alexa Fluor 546 Goat Anti-Mouse IgG (Invitrogen, A11030), Alexa Fluor 488 Goat Anti-Rabbit IgG (Invitrogen, A11034), Alexa Fluor 647 Goat Anti-Rabbit IgG (Invitrogen, A21245). Images were taken by confocal microscopy (Zeiss LSM 800) with same settings across groups. The colocalization of eEF2 with different cell type markers was analyzed by calculating the Manders' Colocalization Coefficients using ImageJ (National Institutes of Health, 1.8.0_172) and the plugin Coloc 2. The Manders' Coefficient corresponds to the fraction of eEF2 (green) overlapping with markers of different cell types (red) divided by the total green signal in an image.

Validation of eEF2 antibody specificity for immunohistochemistry

The experiment procedure was similar to normal immunostaining, except that the primary antibody was first incubated with full-length recombinant eEF2 protein (cusabio, CSB-YP007434MO) as the immunizing blocking agent at 1:5 or 1:10 weight ratio (antibody: blocking protein) for 1 h constant rotation at room temperature, before adding to the brain slice.

FUNCAT and immunofluorescence analysis

Acute brain slices from PFC were prepared as described in SUnSET method. FUNCAT was performed as described previously with minor modifications (Hörnberg *et al*, 2020). Slices (100 μm) from WT and HET mice were incubated with 2 mM AHA (Click

Chemistry, 1066-100) for 4 h. After the incubation, slices were washed using PBS for three times and fixed with 4% paraformaldehyde (PFA) overnight at 4°C. Slices were blocked and permeabilized in 3% BSA, 10% goat serum, and 0.5% Triton X-100 at 37°C for 2 h. After washing 3 × 5 min with 3% BSA in PBS, Click-iT reaction cocktail (Invitrogen, C10269) supplemented with 2 μM alkyne tagged to Alexa 488 (Invitrogen, A10267) was added to slices and incubated overnight at 4°C. Slices were washed with PBS the next day followed by incubation with Anti-CaMKIIα (CST, 50049) at 37°C for 3 h. Alexa Fluor 546 Goat Anti-Mouse IgG was added after slices were washed, then incubated at 37°C for 2 h. DAPI was then added for 15-min incubation and washed, and slices were mounted with Hydromount. Images were taken by confocal fluorescence microscopy (Zeiss LSM 800) with the same settings across groups. ImageJ (National Institutes of Health, 1.8.0_172) was used to analyze the AHA mean intensity in all AHA$^+$ cells or in CaMKIIα$^+$ cells.

SUnSET-based *de novo* protein synthesis measurement

Mice were anesthetized with tribromoethanol (Sigma, T48402) and intracardially perfused with hypertonic dissection buffer (212.7 mM sucrose, 2.6 mM KCl, 1.6 mM NaH_2PO_4, 10 mM $MgCl_2$, 0.5 mM $CaCl_2$, 26 mM $NaHCO_3$, and 10 mM glucose). Brains were removed rapidly and immersed in pre-cold dissection buffer, bubbled with 95% O_2 and 5% CO_2. Slices from PFC, cortex without PFC, and hippocampus were prepared using a vibratome (LEICA VT 1200S) and immediately transferred to bubbled artificial cerebrospinal solution fluid (ACSF, containing 124 mM NaCl, 3 mM KCl, 1.25 mM NaH_2PO_4, 1 mM $MgCl_2$, 2 mM $CaCl_2$, 26 mM $NaHCO_3$, and 10 mM glucose) at 32°C and recovered for at least 1 h. Slices were then incubated with 10 μg/ml puromycin (Millipore, 540411) in bubbled ACSF for 45 min. Slices were homogenized with RIPA followed by Western blot analysis.

Nissl staining

Coronal brain cryosections were prepared similarly as described in the "Immunofluorescence" section. The slices were stained by Nissl Staining Solution (Beyotime) at 37°C for 10 min and washed with deionized water. After soaking in 95% ethanol twice, the slices were dehydrated in 100% ethanol and cleared in xylene. Finally, the slices were coverslipped and imaged with OLYMPUS BX53 microscope then analyzed by ImageJ.

Golgi staining

In brief, the mouse brains were cut into 2–3 mm thickness tissue sections after being fixed. These sections were incubated in Golgi-cox staining solution (Servicebio, G1069) in the dark for 2 weeks at room temperature. Then, the sections were immersed in 80% glacial acetic acid followed by 30% sucrose and subsequently being sectioned into 100 μm slices using a vibrating microtome (Leica VT1200S). Slices were treated with concentrated ammonia water for 15 min, with distilled water for 1 min and acid-hardening fixing solution for 15 min, finally sealed with glycerin gelatin. Neuronal morphology was imaged using bright-field illumination of the Zeiss microscope system (Zeiss Axio Observer). Spine density was analyzed using ImageJ.

LC–MS/MS and data analysis

The PFC crude synaptosome fraction prepared from 3 WT and 3 HET mice was used for the proteomic analysis. Proteins of each sample were precipitated using acetone. After drying, the precipitate was sonicated in Triethylammonium bicarbonate (TEAB) with a final concentration of 200 mM. Proteins were digested by incubating with trypsin at 1:50 trypsin-to-protein m/m overnight at 37°C. To reduce proteins, dithiothreitol (DTT) was added to a final concentration of 5 mM at 56°C for 30 min. Then, iodoacetamide (IAA) was added at the final concentration of 11 mM and incubated for 15 min at room temperature in the dark.

The digested peptides were dissolved in solvent A (0.1% formic acid and 2% acetonitrile) and then separated on an EASY-nLC 1200 UPLC system (ThermoFisher Scientific). Solvent B (0.1% formic acid and 90% acetonitrile) was applied with a liner gradient of 6–80% over 90 min at 500 nl/min flow rate. The peptides were injected into the NSI for ionization followed by analysis in Orbitrap Exploris™ 480 mass spectrometer. The ion source voltage applied was 2.3 kV, and the FAIMS compensation voltage (CV) was −45 V, −65 V. The peptide precursor and its secondary fragments were detected and analyzed by high-resolution Orbitrap. The scanning range was set to 400–1,200 m/z for the primary mass, and the scanning resolution was set at 60,000. The fixed starting point of the secondary mass was 110 m/z, the secondary scanning resolution was set to 15,000, and TurboTMT was set to Off. The data-dependent scanning (DDA) program was used for data acquisition. Automatic gain control (AGC) was set at 5E4 ions/s.

The obtained data were aligned using Proteome Discoverer (v2.4.1.15) against the RefSeq database (Mus_musculus_10090_SP_20210721.fasta, 17,089 sequences). The anti-database was added to calculate the false positive rate (FDR) caused by random matching, and a common contamination library was added to the database to eliminate the influence of contaminating proteins in the identification results. The restriction method was Trypsin (Full). The number of cut sites was 2. The minimum peptide length was set to six amino acid residues. The maximum number of peptide modifications was set to 3. The mass error tolerance of the primary precursor ion was set to 10 ppm, which of the secondary fragment ion was 0.02 Da. Set Carbamidomethyl (C) as a fixed modification, and set Oxidation (M), Acetyl (N-terminus), Met-loss (M), and Met-loss + acetyl (M) as variable modifications. The FDR for protein, peptide, and PSM identification was set to 1%.

The number of proteins quantified by at least two unique peptides was 3,957. The Principal Component Analysis (PCA) was carried out by R 4.1.0. The ratio of the averaged relative quantitative value of each protein in multiple repeated samples is used as the Fold Change (FC). The top 15% proteins of upregulated or downregulated were selected for heatmap generating and Gene Ontology (GO) annotation illustrated by clusterProfiler R package (Wu et al, 2021). GSEA software v4.1.0 was used to identify the significantly enriched specified GO terms (Mootha et al, 2003; Subramanian et al, 2005), with the number of permutations set at 1,000 and permutation type set as gene_set. Expression values were used as phenotype labels and Signal-2-Noise was set as Metrics for Ranking Genes. The P-value and FDR were set at < 0.05 and < 0.25, respectively.

Primary cortical neuron culture

Primary cortical neurons were cultured from E18.5 Sprague Dawley (SD) rat embryos as previously described (Xiao et al, 2013; Huang et al, 2020). Briefly, the cortices were trypsinized to obtain single cell suspension. Cells was seeded onto 18-mm coverslips coated with Poly-D-Lysine (1 mg/ml, Sigma) in 12-well culture plates, at a final density of 2.5×10^4 cells/coverslips, and cultured in Neurobasal Medium (21103049, Gibco) supplemented with 2% B27 (17504044, Gibco), 2 mM L-Glutamine (25030081, Gibco), and 0.06% D-Glucose (A2494001, Gibco).

Lentivirus infection and puromycin-proximity ligation assay (PLA)

Lentivirus (LV)-U6-Eef2 shRNA-CMV-EGFP-WPRE or LV-U6-scramble-CMV-EGFP-WPRE (BrainVTA) was added into the primary cortical neurons (MOI 10) at DIV (days in vitro) 9. The sequence of Eef2 shRNA (from 5′ to 3′) was designed according to a previous report (Gerashchenko et al, 2020): CCGG-CAGCCAAGCTGATC GAGAA-CTCGAG-TTCTCGATCAGCTTGGCTG-TTTTTT. De novo GluA2 was detected at DIV14 by proximity ligation assay (PLA) with puromycin labeling as previously described with minor modifications (tom Dieck et al, 2015; Li & Götz, 2017). Newly synthesized proteins were labeled for 10 min by 1 μM puromycin (Millipore, 540411), followed by quick washes with cold PBS, then neurons were fixed in PFA for 20 min and permeabilized with 0.5% Triton X-100 in PBS for 15 min at room temperature. After being blocked with the Duolink blocking buffer (Sigma, DUO92002) for 1 h at 37°C, neurons were incubated with anti-puromycin (Millipore, MABE342, 1:1,000) and anti-GluA2 (Abcam, ab206293, 1:500) antibodies at 37°C for 1.5 h. Following washes with the Duolink wash buffer (Sigma, DUO82049), PLA probes (Sigma, DUO92002, DUO92004) were applied, and the ligation and amplification (Sigma, DUO92008) steps were performed according to the manufacturer's instructions. The immunostaining of eEF2 or MAP2 after PLA reaction was processed as described in the immunofluorescence method using anti-eEF2 (Abcam, ab75748, 1:500) or anti-MAP2 (Millipore, AB5622, 1:500) antibodies. Images were taken by confocal fluorescence microscopy (Zeiss LSM 800) with the same settings across groups. ImageJ was used to analyze the mean intensity of PLA signals and eEF2 in EGFP^{+} cells.

Electrophysiology

Whole-cell recordings were performed as described previously (Li et al, 2017; Guo et al, 2021). Briefly, mice were anesthetized with isoflurane and transcardially perfused with an ice-cold solution containing the following: (in mM): 212.7 sucrose, 3 KCl, 1.25 NaH_2PO_4, 3 $MgCl_2$, 1 $CaCl_2$, 26 $NaHCO_3$, and 10 dextrose, bubbled with 95% O_2/5% CO_2. Coronal slices from PFC (300 μm) were prepared using a tissue slicer (Vibratome 3000; Vibratome) in ice-cold dissection buffer which is the same as perfusion solution. The slices were immediately transferred to ACSF at 35°C for 30 min before recordings. The recipe of ACSF was similar to the dissection buffer, except that sucrose was replaced with 124 mM NaCl, and the concentrations of $MgCl_2$ and $CaCl_2$ were changed to 1 and 2 mM, respectively. All recordings were performed at 28–30°C. Pyramidal cells in layer 5 of PrL (1.8–2.0 mm from Bregma) were identified visually under

infrared differential interference contrast optics on the basis of their pyramidal somata and prominent apical dendrites. The recordings were obtained using an Integrated Patch-Clamp Amplifier (Sutter Instrument, Novato, CA, USA) controlled by Igor 7 software (WaveMetrics, Portland, OR, USA) filtered at 5 kHz and sampled at 20 kHz. Igor 7 software was also used for acquisition and analysis. The detailed procedures of electrophysiology experiments are as follows.

mEPSCs
To isolate AMPAR-mediated mEPSCs from pyramidal cells in layer 5 of PrL, 1 μM TTX, 20 μM bicuculline, and 100 μM D, L-APV were added to the ACSF which was continually bubbled with 95% O_2/5% CO_2. mEPSCs were recorded at a holding potential (Vh) of −70 mV. Acquired mEPSCs were analyzed using the Mini Analysis ProgramTM (Synaptosoft). The threshold for detecting mEPSCs was set at three times the root mean square (RMS) noise. There was no significant difference in RMS noise between the WT and HET neurons. For the computation of kinetic parameters, 200–300 fully isolated events of mEPSCs were averaged.

Cell excitability
To measure the cell excitability of layer 5 neurons, whole-cell recordings were performed in current-clamp mode at −60 mV. Patch pipettes (2–4 mΩ) were filled with the internal solution consisting of the following (in mM): 130 K-gluconate, 10 KCl, 10 HEPES, 0.5 Na_3GTP, 4 MgATP, 10 Na-phosphocreatine, and 0.2% biocytin, pH 7.2–7.4. The osmolarity was 275–290 mOsm. Spikes were induced by incrementally increasing the current injection (each step increase was 50 pA).

Evoked EPSCs
Evoked EPSCs were recorded from Layer 5 pyramidal cells in the voltage-clamp method. A concentric bipolar stimulating electrode with a tip diameter of 125 μm (FHC) was placed in layer 2/3 to evoke excitatory responses onto pyramidal cells in layer 5. The AMPAR- and NMDAR-mediated current ratio was recorded in the presence of 50 μM PTX at holding membrane potentials of −70 and +40 mV in the same cell with the same internal solution as in the recording for input–output response of AMPAR-mediated EPSCs (below), The AMPAR/NMDAR ratio was calculated as the ratio of the average EPSC peak amplitude at −70 mV to the average amplitude of EPSCs recorded at +40 mV (average of 40–50 ms after afferent stimulation).

To measure the input–output response of AMPAR-mediated EPSCs, Patch pipettes (2–4 mΩ) were filled with the internal solution consisting of the following (in mM): 120 Cs-methylsulfonate, 10 HEPES, 10 Na-phosphocreatine, 5 lidocaine N-ethyl bromide (QX-314), 4 ATP, 0.5 GTP, pH 7.2–7.3; the osmolarity of the solution was 270–285 mOsm. The cell membrane potential was held at −70 mV, and recordings were performed in the presence of 50 μM APV and 100 μM PTX. AMPAR-EPSCs were evoked by a pulse electrical stimulus (0.1 ms width) with different stimulus intensities systematically (5, 10, 15, 20, 25, 30, 40, 60, and 80 μA). At least 10 responses for each intensity were averaged to measure the currents of AMPAR-EPSCs. Only cells with series resistance < 20 mΩ and input resistance > 100 mΩ were studied.

E/I balance measurement
To measure E/I balance, evoked EPSC and evoked IPSC were recorded in the same cell in layer 5 of PrL. To isolate combined AMPAR/NMDAR-mediated currents, neurons were held at the reversal potential for $GABA_A$R-mediated currents. To isolate $GABA_A$R-mediated currents, neurons were held at the reversal potential for AMPAR/NMDAR-mediated currents. The reversal potentials for each neuron were determined by holding the membrane potential from −85 to −65 mV in 5 mV increments for $GABA_A$R and from −10 to +10 mV in 5 mV increments for AMPAR/NMDAR. The average reversal potentials for EPSCs (WT: 2.625 ± 1.438 mV, $n = 8$; HET: 4.375 ± 1.752 mV, $n = 8$; $P = 0.4529$) and IPSCs (WT: -71.29 ± 1.085 mV, $n = 7$; KO: -69.57 ± 1.913 mV, $n = 7$; $P = 0.4508$) were not different between WT and HET mice, and at least 10 responses for the stimulus intensity to evoke the maximal amplitudes of EPSCs and IPSCs were averaged to measure the E/I ratio.

Inward rectification of AMPAR-current
For generating current–voltage (I–V) curves for rectification measurements, cells were held at −80, −60, −40, −20, 0, +20, and +40 mV. Patch pipettes (2–4 mΩ) were filled with the internal solution consisting of the following (in mM): 90 Cs-methanesulfonate, 5 $MgCl_2$, 8 NaCl, 10 EGTA, 20 HEPES, 1 QX-314, 2 MgATP, 0.5 Na_3GTP, and 0.2 spermine, pH 7.2 with CsOH. For the measurement of the I–V curve and the rectification index (RI), the NMDAR antagonist AP-5 (50 μM) and the $GABA_A$R antagonist bicuculline (20 μM) were present in the ACSF. Inward rectification was calculated by dividing the amplitude of average EPSC measured at −60 mV by that at +40 mV. There were no significant differences in calculated reversal potentials between groups (WT: 3.45 ± 3.7 mV, $n = 11$; HET: 2.8 ± 3.8 mV, $n = 12$; $P = 0.4937$, unpaired t test). Reversal potentials were calculated using equations generated by fitting a linear regression curve to the current values collected at negative holding potentials.

Behavior tests

Mice were housed in three or four per cage at $23 \pm 2°C$ in a 12 h light/dark cycle (light on/off at 8:00 am/ 20:00 pm), with *ad-lib* access to water and food. For the recording of pup USVs, pup littermates of both sexes of *Eef2* WT and HET were used. For the tests of adult mice, experiments were performed using age-matched (3–5 months) littermates of both sexes of *Eef2* WT and HET mice. Before the beginning of behavior tests, mice were housed individually for at least 4 days and handled 5 min each day for three consecutive days. Before each test, mice were transferred to the test room 1 h for habituation. Experimenters were blind to the genotypes during testing. More behavioral experiments were performed following our previous protocols (Guo *et al*, 2021, 2022; Xiao *et al*, 2021; Yang *et al*, 2021c), and the detailed procedures are described as follows.

USV Recording
Calls emitted by pups during isolation were recorded on postnatal days 3, 6, 9, and 12 as described previously (Yang *et al*, 2021c). Briefly, each pup was isolated from its dam and littermates and placed into a glass beaker with new bedding. The beaker was put

just under the microphone in a sound-proof container. The pup USVs were recorded for 5 min by Avisoft SASLab Pro Recorder. Characteristics of ultrasounds were measured by automatic parameter measurements.

Grooming

The tested mouse was placed in a new, thinly bedded test cage, which was similar to its home cage. Before video recording, each mouse was given a 10-min habitation. The following 20 min was taken for recording the grooming behavior, which was timed manually.

Open-field test

Spontaneous exploration behavior was tested in a white opaque box ($40 \times 40 \times 40$ cm). Each mouse was placed in the center of the box and allowed to explore freely for 30 min. Performances of the mice were recorded by an overhead video camera. The distance of movement was analyzed by Topscan 3.0, Clever Sys Inc.

Marble-burying

The marble-burying test was used to detect repetitive stereotyped behavior of mice. Each mouse was placed into a cage with 4-cm-deep bedding. Twenty black glass marbles (1.5 cm in diameter) were arranged in a rectangular, 4 by 5 array on the surface of bedding. The mouse was placed in the testing cage from one side without touching the marbles, then allowed to explore and dig for 20 min. A marble that was at least two-thirds under the bedding was considered as a buried marble.

Three-chamber test

Social approach and social novelty were measured in a 60 cm (length) $\times$ 40 cm (width) $\times$ 20 cm (height) opaque white box as described previously (Guo *et al*, 2021). Briefly, the test mouse was placed into the middle chamber and allowed to freely explore the three chambers for 10 min to habituate. To perform the social approach test, an empty wire mesh cup was placed in one outer corner of one side chamber. A similar cup with an unfamiliar mouse (stranger #1) was placed in the diagonally opposite corner of the other side chamber. The test mouse was allowed to explore either the empty cup or the stranger mouse-contained cup for 10 min. In the social novelty phase, another novel mouse (strange #2) was put into the empty cup, and the test mouse was allowed to explore freely for another 10 min. The time for sniffing the strangers or the empty cup was analyzed using Topscan 3.0. The discrimination score of social approach and social novelty was calculated as below:

Social approach score = time difference on sniffing stranger #1 and empty cup/total time on sniffing stranger #1 and empty cup.

Social novelty score = time difference on sniffing stranger #2 and #1/total time on sniffing stranger #2 and #1.

Tube test

The social dominance was measured by the tube test as described (Fan *et al*, 2019). A 30-cm-long transparent Plexiglas tube with an inside diameter of 30 or 26 mm was used for testing adult male or female mice, respectively. The tube was fixed in the center of an opaque white box. WT and HET mice of same sex and weight differences < 15% were paired to test. Each mouse was tested against all paired opponents from the other genotype, and mice that could not be matched in more than three pairs were excluded. Two days

before the test, mice were trained to go through the tube for five successful passes from each side per day. On the test day, mice were placed at the opposite ends of the tube, with their tails holding by the experimenter until both mice meet in the middle of the tube. The mouse that retreated from the tube first with all four paws out was the loser, and the other one that remained in the tube was the winner.

Elevated zero-maze

The elevated zero-maze test was performed as described to monitor anxiety-like behavior (Guo *et al*, 2021). Each mouse was placed in one of the four junctions of opened and closed quadrants randomly and monitored for 5 min recorded by an overhead video camera. The videos were analyzed using TopScan 3.0.

Nesting

The experiments were performed as described previously with minor modifications (Deacon, 2006). A pressed cotton square nesting material (Nestlet, Ancare) weighing 3 g was provided to each mouse as a new bedding 1 h before the light off. On the next morning, after 1 h of the light on, the nests were evaluated and all the untorn materials were weighed. A rating score (ranging 1–5, where 5 is the best) was assigned to each mouse according to the quality of the nests.

Novel object recognition

The novel object recognition test was carried out as described previously (Bevins & Besheer, 2006). In brief, during the habituation session, mice were habituated individually in the open-field arena for 10 min. One hour later, in the training session, two identical objects (white plastic round bottle caps, 4 cm in diameter and 2.8 cm in height) were fixed on the bottom of the arena, 30 cm apart from each other. Mice were allowed to recognize the objects for 10 min. One day later, a 10-min test session was performed, during which one of the identical objects was replaced by a novel object (a Lego structure, $4.6 \times 2.2 \times 3.5$ cm). The travel distance and the time spent sniffing each object were analyzed by Topscan 3.0.

Y-maze working memory

The Y-shaped maze contains three identical arms (34 cm long, 8 cm wide, and 14 cm deep) marked as A, B, and C. Each mouse was placed at the end of one of the three arms randomly to begin the spatial working memory test. The total number and the order of arm entries were recorded during an 8-min test. To count one arm entrance, all four limbs of the mouse must enter the arm. The spontaneous alteration among three arms was defined as nonoverlapping entrance sequences (i.e., ABC, ACB, CAB, etc.). The percentage of the spontaneous alteration was calculated according to the following formula: Alternation (%) = [number of actual alternations/maximum number of alternations in theory (total number of arm entries-2)] $\times$ 100%.

Forced-swim test

The depression-like behavior was tested by a forced-swim test as previously described (Xiao *et al*, 2021). Four mice were tested simultaneously in an opaque white compartment (66.7 cm long, 16 cm wide, and 26 cm high), which is equally divided into four parts, each containing a clear Plexiglas cylindrical container. The

cylindrical containers are 26 cm high, 16 cm in diameter, and filled with 2 liters of water (24 ± 1°C). Each mouse was gently placed in the center of the cylinder and allowed to swim freely for 6 min. The first 2 min was for habituation, and the final 4 min was used for evaluation. At the end of the test, mice were removed from the cylinders and put back in home cages with a paper towel to dry off. The time of four types of movement including immobility, escaping, climbing, and swimming was analyzed by TopScan 3.0.

Stereotaxic virus injection

Mice were anesthetized with 1.25% tribromoethanol and secured in a stereotaxic apparatus (RWD Life Science). Skull holes were drilled bilaterally and 200 nl of recombinant adeno-associated virus for each side were injected into mPFC: at AP 1.9 mm, LM ± 0.4 mm, DV −1.62 mm (left), −1.60 mm (right) for male mice, and AP 1.8 mm, LM ± 0.4 mm, DV −1.59 mm (left), −1.57 mm (right) for female mice. For the knockdown of *Eef2*, AAV-CMV-DIO-(EGFP-U6)-*Eef2* shRNA-WPRE-hGH polyA or the control virus AAV-CMV-DIO-(EGFP-U6)-scramble-WPRE-hGH polyA (3.10×10^{12} vg/ml, BrainVTA) was injected into bilateral mPFC of CaMKIIα-Cre mice at a rate of 40 nl/min. Mice were subjected to behavior tests 4 weeks after viral injection. For DREADDs-based chemogenetics, rAAV-CaMKIIα-hM3D$_{Gq}$-EGFP-WPRE-hGH polyA (1.376×10^{12} vg/ml, PT-0525, BrainVTA) were injected into bilateral mPFC of *Eef2* HET mice at a rate of 20 nl/min. Two weeks later, the infected excitatory neurons were activated by oral administration of 0.025 mg/ml CNO (TargetMol, T4494) in drinking water for 2 weeks (Phillips *et al*, 2019), whereas the control mice were given normal drinking water, followed by behavior tests.

Drug preparation and treatment

For intraperitoneal injection of PF-4778574 (Sigma, PZ0211), the drug was dissolved in DMSO at a stock concentration of 0.6 mg/ml, which was diluted in saline to a working concentration of 0.03 mg/ml before use. A single dose of 0.3 mg/kg body weight of PF-4778574 or equal volume vehicle (5% DMSO in 0.9% saline) was intraperitoneally injected into *Eef2* HET mice. Three-chamber test was performed 30 min later. For local administration of PF-4778574 in mPFC, a 26-gauge, double guide cannula (RWD Life Science, 62023) was bilaterally implanted into the mPFC of HET mice at AP 1.9 mm, LM ± 0.4 mm, DV −1.60 mm for male mice, and AP 1.8 mm, LM ± 0.4 mm, DV −1.58 mm for female mice. After 7-day recovery, 200 nl PF-4778574 (20 μM in 0.9% saline containing 2‰ DMSO) or vehicle was infused at a rate of 40 nl/min through a 26-gauge double injector cannula (RWD Life Science, 62223), and the injector cannula was then remained for an additional 5 min before removal. Mice were subjected to the three-chamber test 30 min later.

Statistical analysis

All Data except electrophysiological parts were analyzed using GraphPad Prism 8.0. Normal distribution tests were performed, followed by the *F* test to compare variances. For comparisons between two groups, data with non-normal distribution was analyzed by the nonparametric Mann–Whitney test. For normal distributed data from two groups, those with similar SD revealed in the *F* test was analyzed by a paired or unpaired two-tailed *t* test, and those who have significant various SD were analyzed by the Welch's *t* test or the nonparametric Kolmogorov–Smirnov test. One-way or two-way analysis of variance (ANOVA) with the Bonferroni's multiple comparison test was used for multigroup comparisons. For electrophysiological data, all statistical analyses were performed in GraphPad Prism 6.0 and SPSS 21.0. The normality test was performed by the Shapiro–Wilk test. The homogeneity of variance test was performed by the Levene's test. Data that met these two conditions were analyzed using a two-tailed unpaired or paired *t* test, ANOVA, or repeated-measures ANOVA followed by the Tukey's multiple comparison test. Values are expressed as mean ± s.e.m., and $P < 0.05$ is regarded as a statistically significant difference.

Data availability

The mass spectrometry proteomics data have been deposited to the ProteomeXchange Consortium via the PRIDE (Perez-Riverol *et al*, 2022) partner repository with the dataset identifier PXD034864 (https://www.ebi.ac.uk/pride/archive/projects/PXD034864).

Expanded View for this article is available online.

Author contributions

Xuanyue Ma: Data curation; formal analysis; validation; investigation; methodology; writing – original draft; writing – review and editing. **Liuren Li:** Conceptualization; data curation; formal analysis; validation; investigation; methodology; writing – original draft; writing – review and editing. **Ziming Li:** Data curation; validation; investigation; methodology. **Zhengyi Huang:** Data curation; validation; investigation. **Yaorong Yang:** Data curation; validation; investigation; methodology. **Peng Liu:** Data curation; software; investigation; methodology. **Daji Guo:** Validation; investigation; methodology. **Yueyao Li:** Validation; investigation. **Tianying Wu:** Validation; investigation. **Ruixiang Luo:** Validation; investigation. **Junyu Xu:** Methodology. **Wen-Cai Ye:** Resources; data curation; supervision; project administration; writing – review and editing. **Bin Jiang:** Conceptualization; data curation; formal analysis; supervision; funding acquisition; investigation; methodology; writing – original draft; project administration. **Lei Shi:** Conceptualization; resources; data curation; supervision; funding acquisition; validation; investigation; methodology; writing – original draft; project administration; writing – review and editing.

Disclosure and competing interests statement
The authors declare that they have no conflict of interest.

References

Adaikkan C, Taha E, Barrera I, David O, Rosenblum K (2018) Calcium/calmodulin-dependent protein kinase II and eukaryotic elongation factor 2 kinase pathways mediate the antidepressant action of ketamine. *Biol Psychiatry* 84: 65–75

Beckelman BC, Yang W, Kasica NP, Zimmermann HR, Zhou X, Keene CD, Ryazanov AG, Ma T (2019) Genetic reduction of eEF2 kinase alleviates pathophysiology in Alzheimer's disease model mice. *J Clin Invest* 129: 820–833

Bevins RA, Besheer J (2006) Object recognition in rats and mice: a one-trial non-matching-to-sample learning task to study 'recognition memory'. *Nat Protoc* 1: 1306–1311

Cao W, Lin S, Xia QQ, Du YL, Yang Q, Zhang MY, Lu YQ, Xu J, Duan SM, Xia J *et al* (2018) Gamma oscillation dysfunction in mPFC leads to social deficits in neuroligin 3 R451C knockin mice. *Neuron* 98: 670

Chini M, Hanganu-Opatz IL (2021) Prefrontal cortex development in health and disease: lessons from rodents and humans. *Trends Neurosci* 44: 227–240

Collins JE, White RJ, Staudt N, Sealy IM, Packham I, Wali N, Tudor C, Mazzeo C, Green A, Siragher E *et al* (2019) Common and distinct transcriptional signatures of mammalian embryonic lethality. *Nat Commun* 10: 2792

Cook D, Nuro E, Jones EV, Altimimi HF, Farmer WT, Gandin V, Hanna E, Zong R, Barbon A, Nelson DL *et al* (2014) FXR1P limits long-term memory, long-lasting synaptic potentiation, and de novo GluA2 translation. *Cell Rep* 9: 1402–1416

David O, Barrera I, Gould N, Gal-Ben-Ari S, Rosenblum K (2020) D1 dopamine receptor activation induces neuronal eEF2 pathway-dependent protein synthesis. *Front Mol Neurosci* 13: 67

Davies FC, Hope JE, McLachlan F, Nunez F, Doig J, Bengani H, Smith C, Abbott CM (2017) Biallelic mutations in the gene encoding eEF1A2 cause seizures and sudden death in F0 mice. *Sci Rep* 7: 46019

Deacon RM (2006) Assessing nest building in mice. *Nat Protoc* 1: 1117–1119

Delaidelli A, Jan A, Herms J, Sorensen PH (2019) Translational control in brain pathologies: biological significance and therapeutic opportunities. *Acta Neuropathol* 137: 535–555

Domínguez-Iturza N, Lo AC, Shah D, Armendáriz M, Vannelli A, Mercaldo V, Trusel M, Li KW, Gastaldo D, Santos AR *et al* (2019) The autism- and schizophrenia-associated protein CYFIP1 regulates bilateral brain connectivity and behaviour. *Nat Commun* 10: 3454

Dong Z, Chen W, Chen C, Wang H, Cui W, Tan Z, Robinson H, Gao N, Luo B, Zhang L *et al* (2020) CUL3 deficiency causes social deficits and anxiety-like behaviors by impairing excitation-inhibition balance through the promotion of cap-dependent translation. *Neuron* 105: 475–490

Fan Z, Zhu H, Zhou T, Wang S, Wu Y, Hu H (2019) Using the tube test to measure social hierarchy in mice. *Nat Protoc* 14: 819–831

Gerashchenko MV, Nesterchuk MV, Smekalova EM, Paulo JA, Kowalski PS, Akulich KA, Bogorad R, Dmitriev SE, Gygi S, Zatsepin T *et al* (2020) Translation elongation factor 2 depletion by siRNA in mouse liver leads to mTOR-independent translational upregulation of ribosomal protein genes. *Sci Rep* 10: 15473

Ghosh Dastidar S, Das Sharma S, Chakraborty S, Chattarji S, Bhattacharya A, Muddashetty RS (2020) Distinct regulation of bioenergetics and translation by group I mGluR and NMDAR. *EMBO Rep* 21: e48037

Gosrani SP, Jester HM, Zhou X, Ryazanov AG, Ma T (2020) Repression of eEF2 kinase improves deficits in novel object recognition memory in aged mice. *Neurobiol Aging* 95: 154–160

Guo D, Peng Y, Wang L, Sun X, Wang X, Liang C, Yang X, Li S, Xu J, Ye WC *et al* (2021) Autism-like social deficit generated by Dock4 deficiency is rescued by restoration of Rac1 activity and NMDA receptor function. *Mol Psychiatry* 26: 1505–1519

Guo D, Yang X, Gao M, Chen X, Tang Y, Shen L, Li K, Shi L (2022) Deficiency of autism-related gene dock4 leads to impaired spatial memory and hippocampal function in mice at late middle age. *Cell Mol Neurobiol* https://doi.org/10.1007/s10571-022-01233-4

Hahn ME, Schanz N (2002) The effects of cold, rotation, and genotype on the production of ultrasonic calls in infant mice. *Behav Genet* 32: 267–273

Hahn ME, Karkowski L, Weinreb L, Henry A, Schanz N, Hahn EM (1998) Genetic and developmental influences on infant mouse ultrasonic calling. II. Developmental patterns in the calls of mice 2–12 days of age. *Behav Genet* 28: 315–325

Hawer H, Mendelsohn BA, Mayer K, Kung A, Malhotra A, Tuupanen S, Schleit J, Brinkmann U, Schaffrath R (2020) Diphthamide-deficiency syndrome: a novel human developmental disorder and ribosomopathy. *Eur J Hum Genet* 28: 1497–1508

Heise C, Gardoni F, Culotta L, di Luca M, Verpelli C, Sala C (2014) Elongation factor-2 phosphorylation in dendrites and the regulation of dendritic mRNA translation in neurons. *Front Cell Neurosci* 8: 35

Heise C, Taha E, Murru L, Ponzoni L, Cattaneo A, Guarnieri FC, Montani C, Mossa A, Vezzoli E, Ippolito G *et al* (2017) eEF2K/eEF2 pathway controls the excitation/inhibition balance and susceptibility to epileptic seizures. *Cereb Cortex* 27: 2226–2248

Hekman KE, Yu GY, Brown CD, Zhu H, Du X, Gervin K, Undlien DE, Peterson A, Stevanin G, Clark HB *et al* (2012) A conserved eEF2 coding variant in SCA26 leads to loss of translational fidelity and increased susceptibility to proteostatic insult. *Hum Mol Genet* 21: 5472–5483

Holt CE, Martin KC, Schuman EM (2019) Local translation in neurons: visualization and function. *Nat Struct Mol Biol* 26: 557–566

Hörnberg H, Pérez-Garci E, Schreiner D, Hatstatt-Burklé L, Magara F, Baudouin S, Matter A, Nacro K, Pecho-Vrieseling E, Scheiffele P (2020) Rescue of oxytocin response and social behaviour in a mouse model of autism. *Nature* 584: 252–256

Huang M, Liang C, Li S, Zhang J, Guo D, Zhao B, Liu Y, Peng Y, Xu J, Liu W *et al* (2020) Two autism/dyslexia linked variations of DOCK4 disrupt the gene function on Rac1/Rap1 activation, neurite outgrowth, and synapse development. *Front Cell Neurosci* 13: 577

Jabarin R, Levy N, Abergel Y, Berman JH, Zag A, Netser S, Levy AP, Wagner S (2021) Pharmacological modulation of AMPA receptors rescues specific impairments in social behavior associated with the A350V Iqsec2 mutation. *Transl Psychiatry* 11: 234

Jacobs SBR, Van Nostrand JL, Bowen ME, Baker JC, Attardi LD (2020) Siva plays a critical role in mouse embryonic development. *Cell Death Differ* 27: 297–309

Jan A, Jansonius B, Delaidelli A, Somasekharan SP, Bhanshali F, Vandal M, Negri GL, Moerman D, MacKenzie I, Calon F *et al* (2017) eEF2K inhibition blocks Abeta42 neurotoxicity by promoting an NRF2 antioxidant response. *Acta Neuropathol* 133: 101–119

Jan A, Jansonius B, Delaidelli A, Bhanshali F, An YA, Ferreira N, Smits LM, Negri GL, Schwamborn JC, Jensen PH *et al* (2018) Activity of translation regulator eukaryotic elongation factor-2 kinase is increased in Parkinson disease brain and its inhibition reduces alpha synuclein toxicity. *Acta Neuropathol Commun* 6: 54

Jia Z, Agopyan N, Miu P, Xiong Z, Henderson J, Gerlai R, Taverna FA, Velumian A, MacDonald J, Carlen P *et al* (1996) Enhanced LTP in mice deficient in the AMPA receptor GluR2. *Neuron* 17: 945–956

Kelly E, Meng F, Fujita H, Morgado F, Kazemi Y, Rice LC, Ren C, Escamilla CO, Gibson JM, Sajadi S *et al* (2020) Regulation of autism-relevant behaviors by cerebellar-prefrontal cortical circuits. *Nat Neurosci* 23: 1102–1110

Laguesse S, Ron D (2020) Protein translation and psychiatric disorders. *Neuroscientist* 26: 21–42

Larcher L, Buratti J, Héron-Longe B, Benzacken B, Pipiras E, Keren B, Delahaye-Duriez A (2020) New evidence that biallelic loss of function in EEF1B2 gene leads to intellectual disability. *Clin Genet* 97: 639–643

Lazaro MT, Taxidis J, Shuman T, Bachmutsky I, Ikrar T, Santos R, Marcello GM, Mylavarapu A, Chandra S, Foreman A *et al* (2019) Reduced prefrontal synaptic connectivity and disturbed oscillatory population dynamics in the CNTNAP2 model of autism. *Cell Rep* 27: 2567–2578

Lee DK, Li SW, Bounni F, Friedman G, Jamali M, Strahs L, Zeliger O, Gabrieli P, Stankovich MA, Demaree J *et al* (2021) Reduced sociability and social agency encoding in adult Shank3-mutant mice are restored through gene re-expression in real time. *Nat Neurosci* 24: 1243–1255

Li C, Götz J (2017) Somatodendritic accumulation of Tau in Alzheimer's disease is promoted by Fyn-mediated local protein translation. *EMBO J* 36: 3120–3138

Li S, Wang L, Tie X, Sohya K, Lin X, Kirkwood A, Jiang B (2017) Brief novel visual experience fundamentally changes synaptic plasticity in the mouse visual cortex. *J Neurosci* 37: 9353–9360

Li L, He C, Jian T, Guo X, Xiao J, Li Y, Chen H, Kang X, Chen H, Duan X (2020) Attenuated link between the medial prefrontal cortex and the amygdala in children with autism spectrum disorder: Evidence from effective connectivity within the social brain. *Prog Neuropsychopharmacol Biol Psychiatry* 111: 110147

Liu Y, Beyer A, Aebersold R (2016) On the dependency of cellular protein levels on mRNA abundance. *Cell* 165: 535–550

Ma T (2021) Roles of eukaryotic elongation factor 2 kinase (eEF2K) in neuronal plasticity, cognition, and Alzheimer disease. *J Neurochem* https://doi.org/10.1111/jnc.15541

McLachlan F, Sires AM, Abbott CM (2019) The role of translation elongation factor eEF1 subunits in neurodevelopmental disorders. *Hum Mutat* 40: 131–141

Mignogna ML, Musardo S, Ranieri G, Gelmini S, Espinosa P, Marra P, Belloli S, Murtaj V, Moresco RM, Bellone C *et al* (2021) RAB39B-mediated trafficking of the GluA2-AMPAR subunit controls dendritic spine maturation and intellectual disability-related behaviour. *Mol Psychiatry* 26: 6531–6549

Mootha VK, Lindgren CM, Eriksson KF, Subramanian A, Sihag S, Lehar J, Puigserver P, Carlsson E, Ridderstråle M, Laurila E *et al* (2003) PGC-1alpha-responsive genes involved in oxidative phosphorylation are coordinately downregulated in human diabetes. *Nat Genet* 34: 267–273

Moritz CP, Mühlhaus T, Tenzer S, Schulenborg T, Friauf E (2019) Poor transcript-protein correlation in the brain: negatively correlating gene products reveal neuronal polarity as a potential cause. *J Neurochem* 149: 582–604

Nabais Sá MJ, Olson AN, Yoon G, Nimmo GAM, Gomez CM, Willemsen MA, Millan F, Schneider A, Pfundt R, de Brouwer APM *et al* (2021) De Novo variants in EEF2 cause a neurodevelopmental disorder with benign external hydrocephalus. *Hum Mol Genet* 29: 3892–3899

Park S, Park JM, Kim S, Kim JA, Shepherd JD, Smith-Hicks CL, Chowdhury S, Kaufmann W, Kuhl D, Ryazanov AG *et al* (2008) Elongation factor 2 and fragile X mental retardation protein control the dynamic translation of Arc/Arg3.1 essential for mGluR-LTD. *Neuron* 59: 70–83

Park Y, Page N, Salamon I, Li D, Rasin MR (2021) Making sense of mRNA landscapes: translation control in neurodevelopment. *Wiley Interdiscip Rev RNA* 13: e1674

Perez-Riverol Y, Bai J, Bandla C, García-Seisdedos D, Hewapathirana S, Kamatchinathan S, Kundu DJ, Prakash A, Frericks-Zipper A, Eisenacher M *et al* (2022) The PRIDE database resources in 2022: a hub for mass spectrometry-based proteomics evidences. *Nucleic Acids Res* 50: D543–D552

Phillips ML, Robinson HA, Pozzo-Miller L (2019) Ventral hippocampal projections to the medial prefrontal cortex regulate social memory. *Elife* 8: e44182

Qin L, Ma K, Yan Z (2019) Chemogenetic activation of prefrontal cortex in shank3-deficient mice ameliorates social deficits, NMDAR hypofunction, and Sgk2 downregulation. *iScience* 17: 24–35

Sacai H, Sakoori K, Konno K, Nagahama K, Suzuki H, Watanabe T, Watanabe M, Uesaka N, Kano M (2020) Autism spectrum disorder-like behavior caused by reduced excitatory synaptic transmission in pyramidal neurons of mouse prefrontal cortex. *Nat Commun* 11: 5140

Salpietro V, Dixon CL, Guo H, Bello OD, Vandrovcova J, Efthymiou S, Maroofian R, Heimer G, Burglen L, Valence S *et al* (2019) AMPA receptor GluA2 subunit defects are a cause of neurodevelopmental disorders. *Nat Commun* 10: 3094

Schwanhäusser B, Busse D, Li N, Dittmar G, Schuchhardt J, Wolf J, Chen W, Selbach M (2011) Global quantification of mammalian gene expression control. *Nature* 473: 337–342

Shaffer CL, Hurst RS, Scialis RJ, Osgood SM, Bryce DK, Hoffmann WE, Lazzaro JT, Hanks AN, Lotarski S, Weber ML *et al* (2013) Positive allosteric modulation of AMPA receptors from efficacy to toxicity: the interspecies exposure-response continuum of the novel potentiator PF-4778574. *J Pharmacol Exp Ther* 347: 212–224

Shen M, Lv D, Li S, Zhang Y, Wang Z, Zhao C, Chen X, Wang C (2019) Positive allosteric modulation of AMPAR by PF-4778574 produced rapid onset antidepressant actions in mice. *Cereb Cortex* 29: 4438–4451

Shen Y, Zhang ZC, Cheng S, Liu A, Zuo J, Xia S, Liu X, Liu W, Jia Z, Xie W *et al* (2021) PQBP1 promotes translational elongation and regulates hippocampal mGluR-LTD by suppressing eEF2 phosphorylation. *Mol Cell* 81: 1425–1438

Sossin WS (2021) *The Oxford handbook of neuronal protein synthesis.* New York, NY: Oxford University Press

Sossin WS, Costa-Mattioli M (2019) Translational control in the brain in health and disease. *Cold Spring Harb Perspect Biol* 11: a032912

Subramanian A, Tamayo P, Mootha VK, Mukherjee S, Ebert BL, Gillette MA, Paulovich A, Pomeroy SL, Golub TR, Lander ES *et al* (2005) Gene set enrichment analysis: a knowledge-based approach for interpreting genome-wide expression profiles. *Proc Natl Acad Sci USA* 102: 15545–15550

Sutton MA, Taylor AM, Ito HT, Pham A, Schuman EM (2007) Postsynaptic decoding of neural activity: eEF2 as a biochemical sensor coupling miniature synaptic transmission to local protein synthesis. *Neuron* 55: 648–661

Taha E, Patil S, Barrera I, Panov J, Khamaisy M, Proud CG, Bramham CR, Rosenblum K (2020) eEF2/eEF2K pathway in the mature dentate gyrus determines neurogenesis level and cognition. *Curr Biol* 30: 3507–3521

Tom Dieck S, Kochen L, Hanus C, Heumüller M, Bartnik I, Nassim-Assir B, Merk K, Mosler T, Garg S, Bunse S *et al* (2015) Direct visualization of newly synthesized target proteins in situ. *Nat Methods* 12: 411–414

Trakoshis S, Martinez-Canada P, Rocchi F, Canella C, You W, Chakrabarti B, Ruigrok AN, Bullmore ET, Suckling J, Markicevic M *et al* (2020) Intrinsic excitation-inhibition imbalance affects medial prefrontal cortex differently in autistic men versus women. *Elife* 9: e55684

Ugur Iseri SA, Yucesan E, Tuncer FN, Calik M, Kesim Y, Altiokka Uzun G, Ozbek U (2019) Biallelic loss of EEF1D function links heat shock response pathway to autosomal recessive intellectual disability. *J Hum Genet* 64: 421–426

Verpelli C, Piccoli G, Zibetti C, Zanchi A, Gardoni F, Huang K, Brambilla D, Di Luca M, Battaglioli E, Sala C (2010) Synaptic activity controls dendritic spine morphology by modulating eEF2-dependent BDNF synthesis. *J Neurosci* 30: 5830–5842

Wang W, Rein B, Zhang F, Tan T, Zhong P, Qin L, Yan Z (2018) Chemogenetic activation of prefrontal cortex rescues synaptic and behavioral deficits in a mouse model of 16p11.2 deletion syndrome. *J Neurosci* 38: 5939–5948

Weng W, Chen Y, Wang M, Zhuang Y, Behnisch T (2016) Potentiation of Schaffer-Collateral CA1 synaptic transmission by eEF2K and p38 MAPK mediated mechanisms. *Front Cell Neurosci* 10: 247

Wu T, Hu E, Xu S, Chen M, Guo P, Dai Z, Feng T, Zhou L, Tang W, Zhan L *et al* (2021) clusterProfiler 4.0: A universal enrichment tool for interpreting omics data. *Innovation* 2: 100141

Xiao Y, Peng Y, Wan J, Tang G, Chen Y, Tang J, Ye WC, Ip NY, Shi L (2013) The atypical guanine nucleotide exchange factor Dock4 regulates neurite differentiation through modulation of Rac1 GTPase and actin dynamics. *J Biol Chem* 288: 20034–20045

Xiao H, Zhang Q, Zhong P, Tang G, Tao L, Huang Z, Guo D, Liao Y, Peng Y, Wu ZL *et al* (2021) Securinine promotes neuronal development and exhibits antidepressant-like effects via mTOR activation. *ACS Chem Nerosci* 12: 3650–3661

Yang CY, Hung YC, Cheng KH, Ling P, Hsu KS (2021a) Loss of CC2D1A in glutamatergic neurons results in autistic-like features in mice. *Neurotherapeutics* 18: 2021–2039

Yang W, Zhou X, Ryazanov AG, Ma T (2021b) Suppression of the kinase for elongation factor 2 alleviates mGluR-LTD impairments in a mouse model of Alzheimer's disease. *Neurobiol Aging* 98: 225–230

Yang X, Guo D, Li K, Shi L (2021c) Altered postnatal developmental patterns of ultrasonic vocalizations in Dock4 knockout mice. *Behav Brain Res* 406: 113232

Yennawar M, White RS, Jensen FE (2019) AMPA receptor dysregulation and therapeutic interventions in a mouse model of CDKL5 deficiency disorder. *J Neurosci* 39: 4814–4828

Zanos P, Gould TD (2018) Mechanisms of ketamine action as an antidepressant. *Mol Psychiatry* 23: 801–811